

# **Implementation of Closed Loop Feedback Control of Piezoelectric Disc based Atomic Force Microscope**

Usman Ali Javid

Supervised by  
Dr. M. Sabieh Anwar

Department of Physics  
Lahore University of Management Sciences

## Acknowledgements

A lot of people have contributed towards the completion of this project. Firstly, my parents have provided me with constant motivation throughout the year and helped arrange so many trips to Lahore. My friends and colleagues have kept my spirits high in times where I felt over-burdened while managing the project in Lahore and classes in Islamabad. Thanks to Salman, Tabinda, Abdullah Lodhi, Ansub, Hisham, Irteza and Asad Raza for keeping me on my toes with their constant support and praise. Special thanks to Ahmer for providing support for fabricating electronics for the project.

Dr. Mashhood Ahmad has been a mentor to me through the entirety of this endeavor. He has not only helped me understand the theory of the project, but constantly guided me in developing research skills and choosing a right path for my future studies. I have acquired a huge amount of knowledge on topics of research in physics in his classes and under his supervision for this project.

Special thanks to Physlab at the department of Physics, LUMS. Physlab is a unique team of scientists and engineers specializing in research and development in experimental physics and physics education. This project has been entirely funded by them and all the support and logistics has been provided in full by Physlab. Thanks to Ali Akbar and Azeem for helping me out and for providing a listening ear whenever I needed someone. Thanks to Dr. Usman for providing his expertise in the field of microscopy. Thanks to Hafiz sahib, Khadim bhai and Ali Hasan for providing hardware support and helping me streamline the project.

The work was originally started by Muhammad Wasif who is a former member of Physlab. He laid most of the ground work for the mechanical and optical design and determining what equipment were needed. He laid a very solid foundation on which I was able to build upon with relative ease. He also has helped me after I took over the project and guided me in getting to know the environment I would be developing the AFM in for the next year.

Ordinarily, this would conclude the acknowledgements but I cannot fathom going forward without mentioning one name and that is Dr. Sabieh Anwar. He is the leader of Physlab and the person behind this and many other high profile physics projects in the country. It is because of him this project exists and has reached so many milestones over these years. Dr. Sabieh has turned an idea of a home grown AFM into a reality. His knowledge of the subject and his insight of design and engineering have no parallel. He has steered this project from scratch to its completion and has provided me with all I have needed to achieve our goals. He has always been there for me for any kind of help including technical, logistics, equipment, and has provided me moral support at every turn. He has given me an environment full of research, scientific enquiry and curiosity. I have learned an immense amount of knowledge from him and it is beyond any doubt that I am a better scientist because of him. I will forever be in his debt.

**DEDICATED TO**

*My Loving Mother*

## **Abstract**

In this project, we have developed an atomic force microscope (AFM) capable of resolving vertical features of the order of 20 nm over an area of 12 microns square. This is achieved by analyzing the reflection of a laser beam off a cantilever making contact with the surface of a sample placed on a motorized translation stage driven by piezoelectric based nano-positioning actuator. The reflected beam's position is monitored by a closed loop proportional-integral control system that was specifically designed for this purpose. This AFM is a cost effective solution for a very sensitive instrument that has become essential in today's research and development in Nanotechnology, Solid State Physics, Microbiology and many other fields of Science and Engineering.

# Contents

Chapter 1 Introduction	
1.1 History of AFM	1
1.2 Working Principle of AFM	2
1.3 Setup of AFM	3
1.4 Applications	4
Chapter 2 Implementing AFM	
2.1 Optical Assembly	9
2.2 Mechanical Construction	12
2.3 Electrical Construction	17
2.4 AFM Operation	21
Chapter 3 Feedback Control of AFM	
3.1 Need for a Feedback Mechanism in AFM Operation	24
3.2 AFM Feedback Loop	24
3.3 Fundamentals of PID Control	26
3.4 Controller Tuning	27
3.5 Performance of AFM with PID control	29
Chapter 4 AFM Imaging	
4.1 Generating AFM Images	33
4.2 Processing AFM Images	34
4.3 AFM Image Artifacts	36
4.4 Actual Images	39
4.5 Further Improvements and Future Directions	45
References	47
Appendices	
Appendix A Software and Codes	50
Appendix B Hardware Support	55

# Chapter 1

## Introduction

### 1.1 History of Atomic Force Microscopy

For most part of scientific history, observing small objects has been done with optical microscopy. Even today, for most practical purposes, these microscopes work effectively. However the resolving power of this technique is cut short by the diffraction limit. In principle a feature that has a size smaller than half the wavelength of illuminating light cannot be resolved. Additional limitations are present due to imperfections of refractive material of the lenses employed and aberrations in images. In the 1980's, scientists started experimenting on a different method to image samples indirectly by measuring the interaction of a small probe when placed on the surface of the sample. This technique is called scanning probe microscopy (SPM). Changes in this interaction could then be used as an image contrast with false colors. First among this class of microscopes was the scanning tunneling microscope (STM) developed in 1982. STM uses Quantum tunneling to create false color image by applying a potential across the probe and the sample. This technique can provide atomic resolution but is limited to conducting samples only. In 1986, another SPM technique was developed that used the atomic forces between a sample atom and the probe to create an image. This came to be known as atomic force microscopy (AFM). At distances beyond 1nm, atomic forces (van der Waals, Electrostatic, capillary forces) take effect and cause the probe to bend in or away from the sample being scanned.

SPM, though an invention of the modern age, has deep roots in how surface profiling has been done in old days. The predecessor of the SPM was the stylus profiler described by Shmalz in 1929 [1], which used a sharp tip on the end of a small bar, to which was dragged along the sample surface, and built up a map, or more often a linear plot, of sample height. This profiler utilized an optical lever to monitor the motion of a sharp probe mounted at the end of a cantilever. A magnified profile of the surface was generated by recording the motion of the stylus on photographic paper. This type of 'microscope' generated profile 'images' with a magnification of greater than 1000x. In 1950, Becker suggested oscillating the probe from an optical lever design used for one of the early models of a surface profiler in the 1920s. This profiler had a vertical resolution of approximately 25 nm [2]. However, a fundamental problem with this sort of instrument persisted, notably that the probe touched the surface in an uncontrolled way, which could lead to probe damage in the case of a hard sample, and sample damage in the case of a soft sample. Either of these problems would reduce the fidelity of the image obtained, as well as the achievable resolution. In 1971 Russell Young demonstrated a non-

contact type of stylus profiler [3]. In his profiler, called the ‘Topografiner’, Young used the fact that the electron field emission current between a sharp metal probe and a surface is extremely dependent on the probe sample distance for electrically conductive samples. This brings us to 1982, when Binnig and Rohner at IBM used this tunneling current to create the first STM [4]. This led to the development of the AFM by measuring atomic forces rather than electrical current to create topographical images of surfaces.

## 1.2 Working Principle of the AFM

Atomic forces between atoms are a function of the distance between them. This concept is exemplified by the Lennard Jones potential function. This potential is developed due to atomic forces between the atoms. Figure 1.1 show the potential plotted versus distance. Starting from a long distance there is no appreciable force. As the distance decreases below 1 nm, an attractive force produces negative potential in the atoms. Further decreasing the distance strengthens the attraction. Due to Quantum effects in the form of Pauli repulsion, an opposite force is also at play. In equation 1.1 the  $r^{12}$  term represents the repulsive force and the  $r^6$  term represents the attractive part. This force-distance relation can be used to detect changes in separation between the sample and probe caused by features on the sample’s surface.

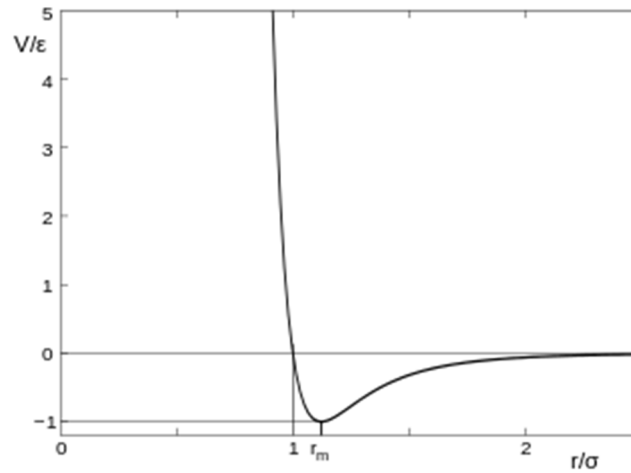


Figure 1.1: Lennard Jones Potential.  $r_m$  represents point of minimum potential.

$$V(r) = 4\epsilon \left[ \frac{\sigma}{r^{12}} + \frac{\sigma}{r^6} \right] \quad (1.1)$$

In (1.1),  $\sigma$  is the distance at which the potential is zero and  $\epsilon$  is the depth of potential well. This equation can be used to determine small distances if the atomic force is known. The resolution of this technique, among other things, will largely depend upon a way to achieve precise and controlled motion of the probe on the sub-nanoscale level. This has been achieved by the development of piezoelectric actuators that can make calculated movements in all axes.

This AFM technique produces three dimensional topological images with contrasts of false colors representing height. This technique can also be used to determine properties such as frictional coefficients, electrical conductivity magnetic properties and several other physical characteristics along with chemical properties and identification of types of atoms present in a given sample.

### 1.3 Setup of AFM

**1. Cantilever** with a sharp tip: The stiffness of the cantilever needs to be less the effective spring constant holding atoms together, which is on the order of 1-10 nN/nm. The tip should have a radius of curvature less than 20-50 nm (smaller is better) and a cone angle between 10-20 degrees.

**2. Scanner:** The movement of the tip or sample in the x, y, and z-directions is controlled by a piezoelectric tube scanner. For typical AFM scanners, the maximum ranges for are 80 mm x 80 mm in the x-y plane and 5 mm for the z-direction.

**3. Detector:** A transducer that can translate the motion of the cantilever into electrical signals. The detectors used in AFM and their techniques are listed in the next section. Figure 1.2 shows a general construction scheme of an AFM.

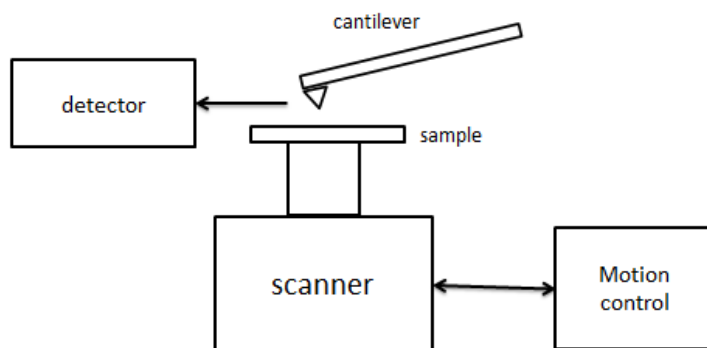


Figure 1.2: A general AFM assembly.

#### 1.3.1 AFM Detection Techniques

Over the years many methods have been used to measure the deflection on the cantilever. They are:

- 1. Laser beam deflection:** the surface features can be quantified by measuring the change in reflection angle of a laser beam focused on top of the cantilever. This technique is called the optical lever and is most commonly used



2. **Interferometry:** The reflection of the laser beam off the cantilever is made to interfere with an undeviated beam in a standard Michelson interferometer setup. The movement of the interference fringes gives the measure of surface features that cause the cantilever deflection [5]. This method, unlike the previous one, needs a check to determine the direction of motion since both up and down motion can cause similar changes in the position of the fringes.
3. **Capacitive Transducers:** Capacitive sensors can be used with one end attached to the probe and the other with the sample. These sensors communicate the distance in terms of changes in their capacitance. This method has a very high sensitivity but it is costly and requires an additional cumbersome mechanical assembly.

### 1.3.2 AFM Operating Modes

AFM can be operated in several ways. The image data can be extracted if the cantilever is in repulsive region of the force distance curve of the attractive. The tip may or may not be driven at a frequency. The different modes of AFM are summarized in this section.

1. **Contact mode:** The cantilever tip is physically in contact with the sample. The tip moves over the surface keeping a constant distance and thus imaging surface features. This mode gives the best resolution but due to dragging, can damage soft samples. This method is not recommended for biological samples
2. **Tapping mode:** The cantilever is driven at near its resonance frequencies. Changes in height alter the amount of force experienced by the oscillating probe which is translated in its amplitude and frequency.
3. **Non-contact mode:** The cantilever hovers over the sample surface at a very small distance. The distance is kept such that the interaction is in the attraction region of the force-distance curve. Changes in distance produce bends in the probe which can then be measured.

## 1.4 Applications

Although AFM, via STM, had its origins in imaging of metals and semiconductors, it was originally invented in order to be able to extend the possibilities of STM to other samples, in particular biological samples. AFM's ability to image a wide variety of samples, coupled with its simplicity of operation and the relatively low cost of the instruments, means that AFM very quickly gained acceptance in an extremely wide range of fields. AFM today has so many applications that the huge diversity cannot possibly be addressed. Here some of the most widely used applications that AFM has today are discussed.

### **1.4.1 Applications in Physics and Material Science**

Fundamental applications in physical sciences include imaging of the fine structure of metals and absorbed species on metals and semiconductors; although this is one area where STM is still more widely applied than AFM, some parameters revealed by AFM can under some circumstances surpass STM. AFM imaging is highly suitable for structural studies of inorganic and organic insulators and has been widely applied.

#### **Surface Roughness at the Nanoscale**

Surface roughness is easy to measure with AFM, due to the fact that AFM produces high contrast on relatively flat surfaces, and produces three-dimensional, digital data by default. AFM gives accurate values for surfaces with roughness down to the level of atomic flatness [6]. Therefore, AFM has become the method of choice to measure nanoscale roughness, and is routinely applied to determine roughness of metals and metal oxides, semiconductors, polymers, composite materials, ceramics, and even biological materials.

#### **Atomic resolution Imaging of Crystal Structures**

The AFM at its atomic resolution allows researchers to observe the atomic structure of a large number of metals, semiconductors, metal oxides, and multi-layered structures [7, 8, 11]. This technique can even reveal sub-atomic detail, e.g. information of molecular orbitals can be determined in some cases [29]. Many atomic-resolution images produced by AFM are produced by non-contact-mode AFM (using FM detection), and often carried out in high-vacuum conditions [10].

#### **Friction Measurements**

Lateral force microscopy (LFM), or friction force microscopy, is applied for many purposes. For example: fundamental study of tribology of macroscopic or atomic scale systems, determination of the friction properties of materials or their characterization [9]. Applications include studies of monolayers, including the friction between monolayers on the probe and on a sample surface [12], friction-based discrimination of phases in polymer blends [13] and discrimination of inclusions in heterogeneous polymer surfaces, and friction studies of carbide coatings for tool coatings. The ability of LFM to discriminate different chemical groups means that it can be used to study phase separation in mixed monolayers [14], and is very commonly used to detect directly deposition of features by dip-pen nanolithography or nanografting, because the contrast is often better than in the height image.

#### **Magnetic Domain Mapping**

Magnetic Force Microscopy (MFM) is a variant of the standard AFM with a magnetic metal coated on the tip of the probe. This specifically allows the measurements of magnetic forces. MFM can create contrast in images based on magnetic activity in the sample. Therefore it is a

very useful tool for imaging magnetic domains in magnetic materials and performing related measurements [15].

## **1.4.2 Applications in Nanotechnology**

### **Imaging Nanoparticles and Nanotubes**

Nanoparticles are probably the most widespread nanostructures, and over the last 10 years or so there has been an enormous increase in the interest in their production due to their unique properties. It is extremely important to have a tool to characterize with extreme accuracy the size of such particles. The AFM is capable of providing more information than just topography, and many other properties of nanoparticles have been probed in recent years [16, 17]. AFM can be used to measure an extremely wide range of nanoparticles including different metal nanoparticles, metal oxide particles, many types of composite metal/organic particles, synthetic polymer particles, biopolymer nanoparticles, nanorods and quantum dots [18] etc.

The mechanical properties of pseudo one-dimensional (1-D) materials such as nanotubes, nanowires, nanorods, nano belts, etc. are the subject of great interest. However, making mechanical measurements of individual nanofibres is extremely difficult, mainly due to the difficulties in locating the objects and fixing them to the testing devices. AFM is ideal for this task, as it can perform both imaging and manipulation of the nanostructures. Furthermore the high positioning accuracy makes it possible to mechanically probe objects having dimensions of less than 10 nm easily [19]. For this reason AFM-based techniques have been widely applied to mechanical measurements of 1-D nanostructures.

### **Nanodevice Construction**

Nanomanipulation, involves assembling tiny building blocks (atoms and molecules) directly, one at a time. Highly complex structures can be formed with this technique. AFM-based systems are well suited to this sort of task, due to the possibility to move the probe with sub-nanometer accuracy. An additional advantage of AFM for this task is the ability to use the instrument as a sensor as well as the manipulator. For example, an AFM-based nanomanipulator with a haptic interface can be used to move carbon nanotubes onto micron-scale electrodes in order to measure their electrical properties [20]. Various biological nanostructures (e.g. DNA, chromosomes, etc.) have been manipulated using AFM probes.

### **Nanoparticle-DNA interactions**

One of the most important areas of nanoscience is Nano bioscience, which can be defined as exploiting nanotechnology to solve biological problems. Within Nano bioscience, probably the most widely applied technology in the medical biosciences is that of nanoparticles, which have been used and proposed for a variety of diagnostic, imaging and treatment strategies. Nanoparticles are almost the sizes of viruses or even of individual proteins, and thus may interact

with the targets as would proteins and viruses. AFM is an ideal technique to directly observe the interaction of nanoparticles (which are usually based on a metal or crystalline semiconductor) with their biomolecule targets [21].

### **1.4.3 Applications in Biology**

#### **Bimolecular Imaging**

Biomolecules form the basis of life, and understanding the structure, function and interactions of biomolecules has been the key to the incredible progress in the life sciences, and medicine in particular. As a technique with sub-molecular resolution and the ability to image soft samples in water, AFM is highly appropriate for the study of a huge range of natural biomolecules. AFM is for example particularly suitable technique for protein studies [22], due to the coupling of high resolution with the ability to study samples under physiological conditions, which is necessary because a protein structure can be highly sensitive to the nature of the proteins' environment. Nucleic acids are also highly suited to AFM imaging, and can be imaged in air and in liquid, and by contact, non-contact and intermittent-contact modes. Samples have included single stranded DNA, double stranded DNA and ssRNA in an extended configuration have been imaged [23].

#### **Bacterial Cell Measurements**

AFM is a highly suitable tool to examine bacteria, and has been widely applied for this purpose. Bacteria are commonly studied by optical microscopy, which can give an overall idea about gross cell morphology, and is also useful for cell-counting studies. In comparison, AFM is slower, and thus is less useful for quantitative cell-counting, but allows measurement of a variety of other cellular properties, particularly by nanoindentation and force spectroscopy experiments [24]. In addition, the greatly increased resolution of AFM allows for the imaging of finer details of cell morphology and sub-cellular features.

#### **Biological Force Spectroscopy**

For the interactions of biological molecules, AFM has some unique advantages. It is very sensitive, allowing the interactions between single pairs of molecules to be studied due to force resolution in the 10 pN range. Moreover, it can be very selective. The control over the x, y and z position of the probe with immobilized molecules means that unlike most techniques, by AFM-based force spectroscopy, it's possible to control exactly which molecules interact, and where they are doing it [25].

# Chapter 2

## Implementing the AFM

This chapter explains the entire structure and design of Physlab's AFM with details on electrical circuitry, data connections, power and signal flow, optics and mechanical design. The AFM project is truly multidisciplinary in nature consisting of an optical assembly along with electronics to drive the data flow and a mechanical setup to support and actuate the system. Figure 1.1 provides the overall design of the AFM with arrows indicating data flow. All information is acquired by the computer through a data acquisition device. The computer also processes the data to generate AFM images.

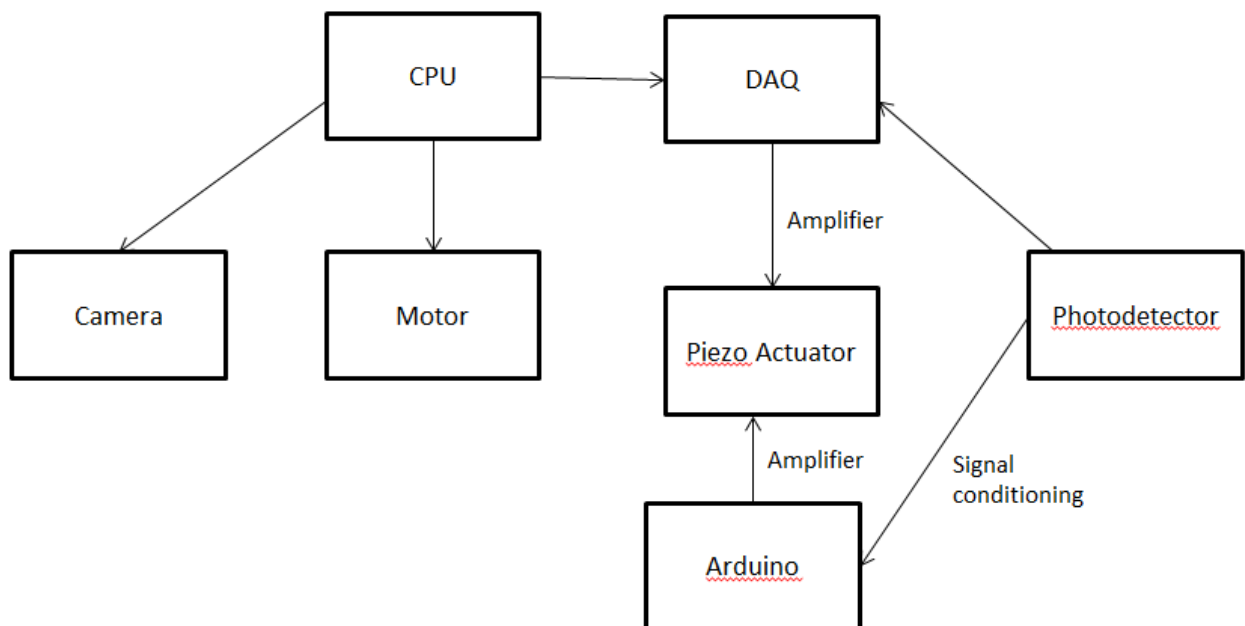


Figure 2.1: AFM flow diagram.

A National Instruments Data Acquisition Board (PCI-6221) is used as the data acquisition device. It is interfaced with a photodetector and an Arduino based microcontroller which will later be used for feedback. The DAQ board also performs the core function of driving the AFM actuator. A LabVIEW program generates the driving signals for the actuator and processes the acquired data from the photodetector. Not involved in the main data flow loop is a CCD Camera

arranged in a digital microscopic arrangement using a 3x microscope objective lens and a precision stepper motor. These two devices are controlled directly by the CPU and are essential for proper functioning of the AFM as will be explained later.

A set of analog electronics control and maintain the data flow and power up the equipment. They are involved in conditioning the data to suit each interfaced component of the AFM. The detailed schematics and working of the electronics are discussed later throughout this chapter. The data from the AFM requires substantial post-processing and we use Matlab for creating the image and a readily available Image processing program “Gwyddion” for processing. The final output is a processed image with measurements of the objects in the field of view.

## 2.1 Optical Assembly

Central to the AFM operation is its optics. Fundamentally an AFM requires a light source, a reflecting probe and a detector capable of measuring change in the reflection angle. A 635nm 1mW Diode Laser is used in the AFM. The laser is collimated with an aspheric lens and then focused sharply onto the top surface of a probe. The power of the light beam after reflection off the probe is measured to be 15uW. The loss of optical power is due to the fact that the focusing lens, despite proper adjustments, cannot make the laser point shorter than the surface of the probe and so, some light is not reflected. Figure 2.1 shows the optical path that the laser takes in the AFM.

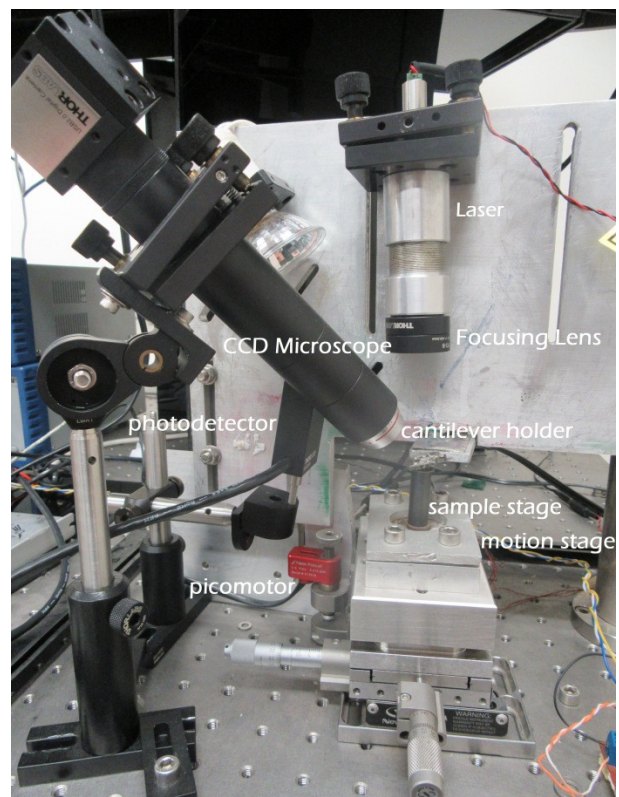
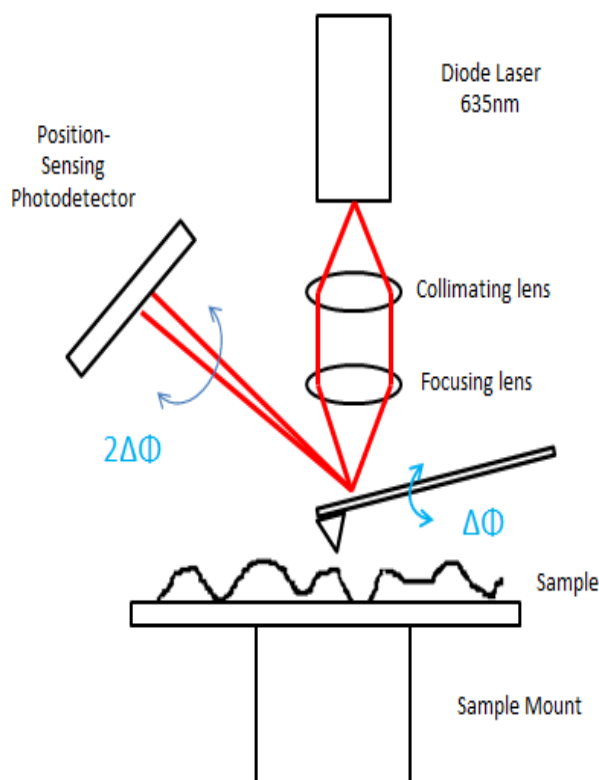


Figure 2.2: AFM optical assembly.

The lenses are placed inside a lens tube which is attached to the diode laser. Also the CCD camera is attached with the objective lens through a similar lens tube. Both elements have adjustment knobs on them to make precise adjustments to the direction and focus of the laser and the field of view of the camera.

### 2.1.1 AFM Probe (Cantilever)

A cantilever is the probe used for scanning the surface that needs to be imaged. A Silicon-nitride probe has been employed in the construction. It has a 31nm pyramidal tip at its bottom. The top surface is gold plated to get good reflection. The entire probe is 220 $\mu$ m long and two of these probes are mounted onto a cantilever of rectangular shape as shown in figure 2.3. Note that the tip is non-magnetic and can only be used to image surface topology.

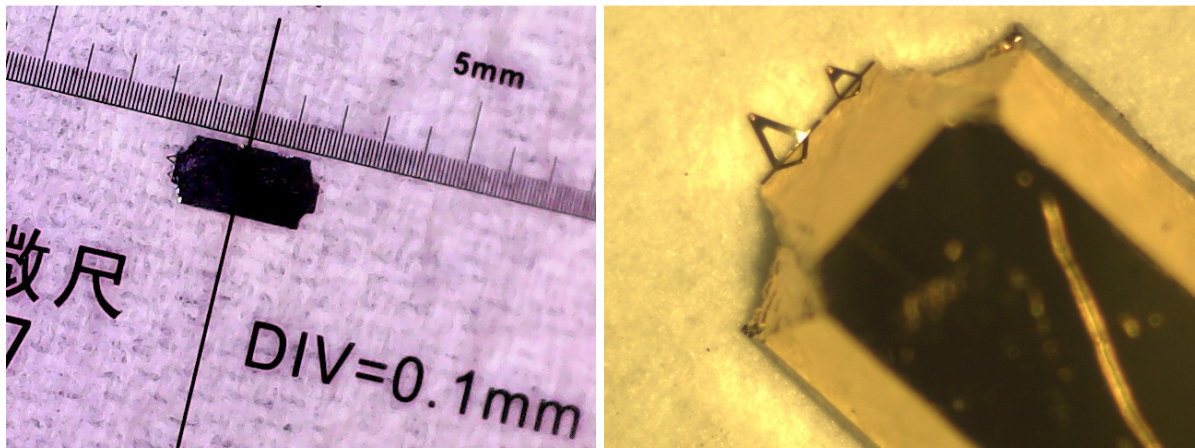


Figure 2.3: cantilever observed through (a) digital Microscope and (b) through CCD microscope.

The cantilever is held in place by a cantilever holder with a clip that firmly grips the probe. The cantilever is flexible and can bend towards and away from the surface of the sample depending upon the atomic force it experiences. The cantilever is a sensitive element and can easily break. So care is taken while loading the cantilever and the process is done under a stereo microscope with special soft edged tweezers.

The cantilever is held by the holder in such a way that it makes an angle with the horizontal. This can be seen in figure 2.2. The laser is shone vertically onto the probe and the reflected beam falls on a photodetector placed in front of the cantilever. By simple geometric calculations, it can be shown that any change in the angle of the cantilever creates a change in the reflection angle of the laser twice its magnitude.

### 2.1.2 Lenses and Tubes

A pair of lenses is present in the path of the laser. The first is an aspheric lens of focal length 1.2 mm. It is used to collimate the light being emitted by the diode. Another lens of focal length 50

mm focuses the light sharply on the surface of the cantilever. The lens is adjusted so that the cantilever is present exactly at its focal point. Both of these lenses are mounted inside a hollow lens tube. A 3x microscope objective connected with a CCD camera is also present to serve as a digital microscope to view the AFM operation and make sure the laser is hitting at the right spot. This microscope has a field of view of approximately 1 x 2  $\mu\text{m}$ .

### 2.1.3 Photodetector

The AFM requires an unusual type of detector that measures the reflection angle of a light beam in addition to its intensity. The detector used in our work is a Thorlabs PDQ80A Quadrant Position Sensing Detector (PSD). It consists of four quadrants of photosensitive semiconductor material. The detector can identify changes in the horizontal and vertical direction by measuring intensities in each quadrant using these formulae for determining normalized coordinates of the laser represented by  $X_p$  and  $Y_p$ .

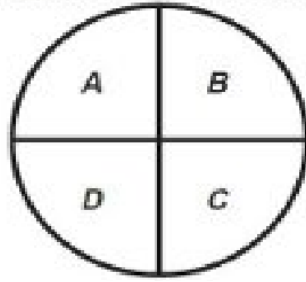


Figure 2.4: Quadrant photodetector.

The normalized  $X_p$  and  $Y_p$  coordinates of a laser spot in the surface of the detector are given by equation 2.1.

$$X_p = \frac{A+D-(B+C)}{A+B+C+D} \quad Y_p = \frac{A+B-(C+D)}{A+B+C+D} \quad \dots\dots\dots (2.1)$$

The photodetector performs a current-to-voltage conversion with its in-built trans-impedance amplifiers with a gain of 10KV per ampere. Its nominal sensitivity at the 635nm wavelength is 0.4A per watt of optical power. A three channel analog output provides the coordinates x, y and a sum of the intensities at each quadrant. Manipulating this data can also give diagonal variations in beam's position.

Figure 2.5 shows the output of the quadrant detector when incident with a 635nm 50uW laser. The dark current was also observed and plotted. This data is used to calculate the Signal to Noise Ratio (SNR) of the detector which will later give a measure of uncertainties in the measurement of image features.



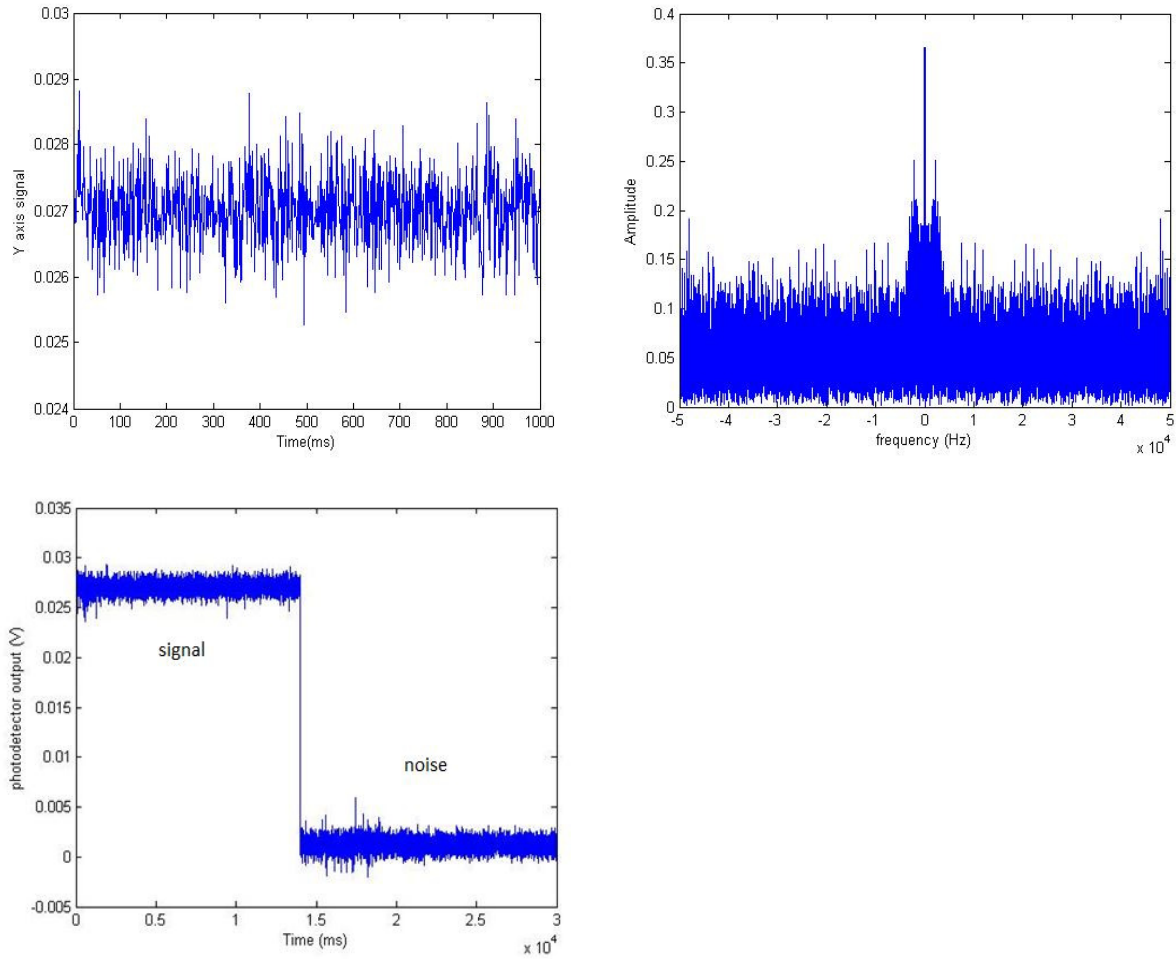


Figure 2.5: (a) Photodetector's output at 50 $\mu$ W 635nm laser beam, (b) its frequency spectrum and (c) comparison of signal and dark current noise.

The adjustment of the photodetector is a critical part of the AFM operation. The laser spot on its surface should be ideally about 5mm in diameter. A larger spot will make it difficult to identify small changes in the reflection angle.

## 2.2 Mechanical Construction

Owing to precise optical adjustments, the setup is constructed on an optical bench with the laser and detector looking downward towards the cantilever. Beneath the cantilever is a sample stage consisting of a precision XYZ motion stage, a sample mount and a sample disc holder which holds the material to be scanned. Each component of the assembly is discussed separately.

### 2.2.1 Precision XYZ motion stage

A Newport ULTRAlign Precision XYZ Linear Translation Stage is at the center of the assembly. It has coarse micrometer level adjustments for X and Y axis and a place to attach a precision motor for Z axis motion. The stage allows controllable linear motion in all axes making it easy to adjust the sample that needs to be scanned.

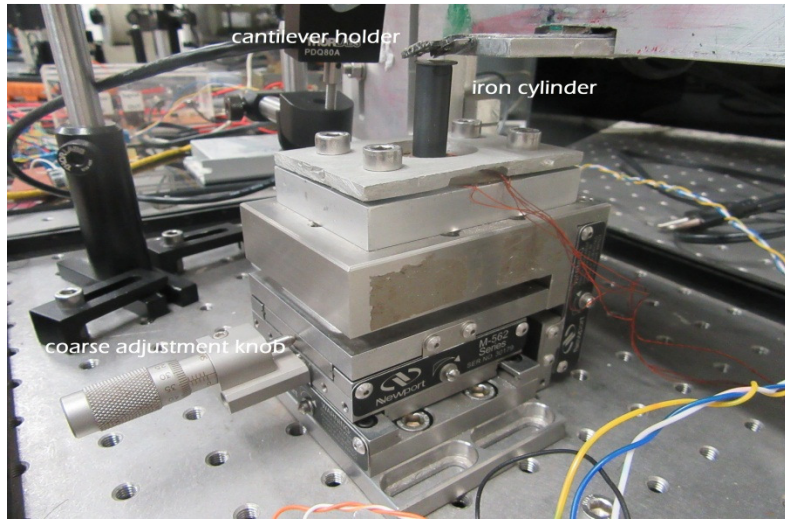


Figure 2.4: Newport Precision XYZ motion Stage.

At the top of the stage is placed a magnetic iron cylinder which serves as the sample mount and holds a magnetic sample disc.

### 2.2.2 Precise Z axis Motion

In order for the AFM to begin operation, the tip needs to be engaged with the surface of the sample. This is an extremely delicate process and requires a slow controlled upward motion of the sample. For this purpose a precision motor is used for a nano-scale Z axis motion.

A Newfocus Picomotor is used for controlled Z axis motion of the stage. This motor can produce a minimum step of size shorter than 30nm. When a sample is mounted and aligned, the motor brings it close enough to the tip that the atomic forces come into play. Thus motor plays the role of adjusting the point of operation on the force distance curve (figure 1.1).

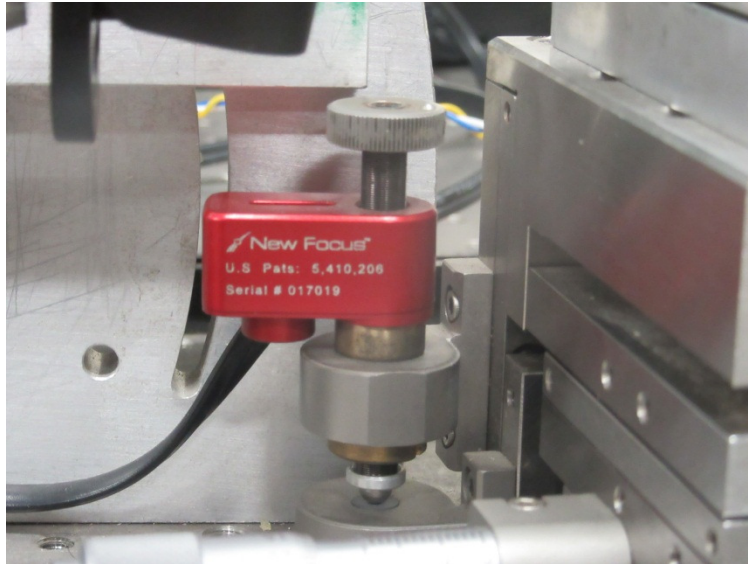


Figure 2.5: New Focus picomotor.

### 2.2.3 Piezoelectric Actuator

The advent of piezoelectric materials has made possible applications that require nano-scale motion. They have played a central role in the development of scanning probe microscopy and eventually the AFM. Traditionally an AFM uses a three dimensional tube made from Piezoelectric material specifically fabricated for this purpose. Such actuators are pre-calibrated from the manufacturer and make up a large percentage of the total cost of the microscope. Since one of the main objectives of this project is to cut the cost it takes to build an AFM, a non-conventional actuator is used.

Piezoelectric discs are commonly used in buzzers since they can vibrate with amplitudes in sub-micrometers. This ability is exploited to turn this disc into an actuator which functions thus:

- A voltage difference created horizontally causes sideways motion of the disc which moves in a bow-like manner
- A voltage difference applied between the top and bottom surface causes the disc to rise and fall at the center causing a linear z axis motion. These types of motion are shown in figure 2.6.

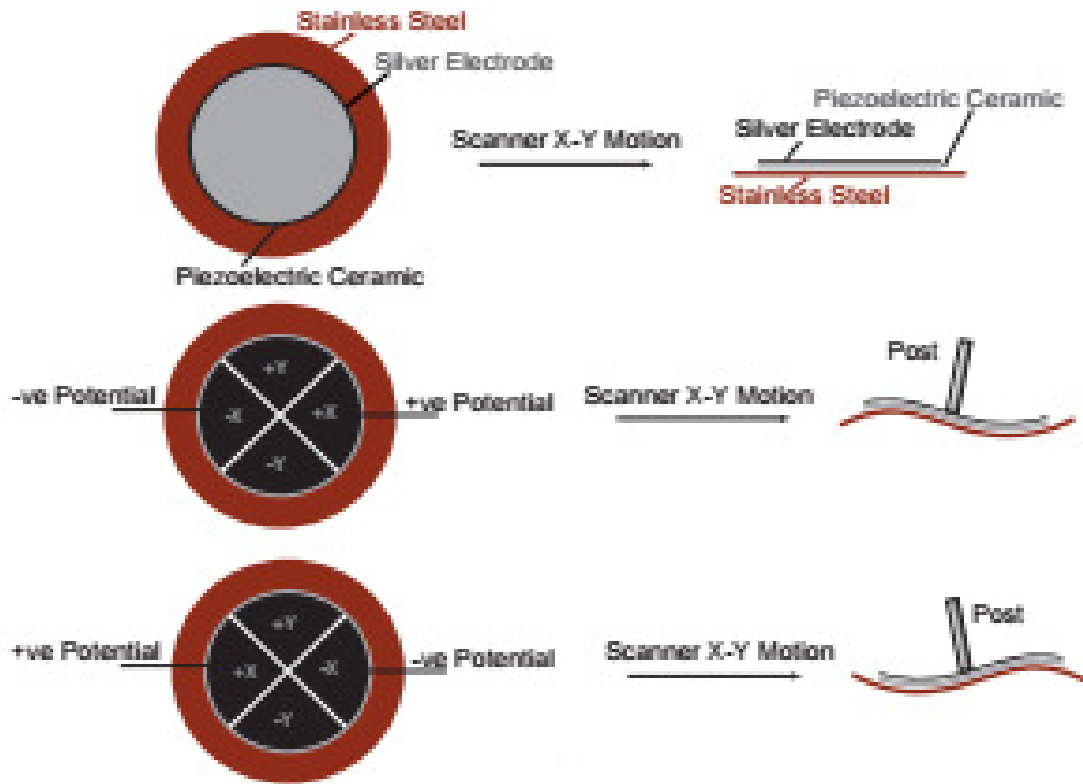


Figure 2.6: Nano-scale Motion with Piezoelectric Discs. Image taken from [5].

To make this happen, a metallic plate on the top surface of the piezoelectric disc is sliced into four quadrants and each of these is connected to the driver electronics. Since motion in all three axes is required, another piezoelectric disc is stacked beneath this disc. The lower disc is used for motion in Z axis with two electrodes connected to its top and bottom surface. This complete actuator is then placed on the motion stage under a metallic plate with a circular opening at the center to provide space to place the sample holder. Figure 2.7 shows a schematic of the piezo actuator assembly.

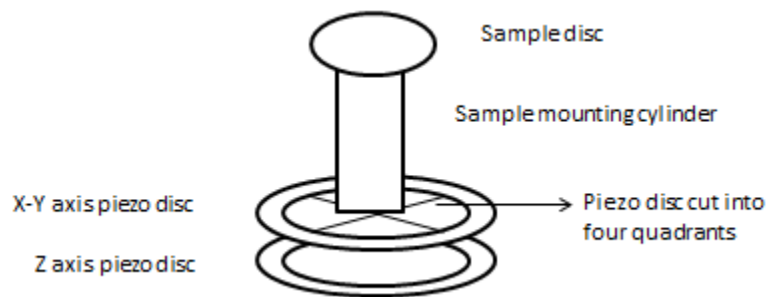


Figure 2.7 Piezo actuator setup.

## 2.2.4 Levels of motional adjustment

To sum up, there are three levels of notional adjustments that can be made to the AFM.

- 1) Coarse Adjustment: The motion stage provides micrometer level adjustments in the x-y direction with its two screw gauges.
- 2) The Precision Picomotor provides a very fine z axis adjustment on the order of nanometers
- 3) The Piezoelectric disc provides sub-nanometer precise motion in all three axes.

All of these degree of freedom play a role in setting the AFM's tip-sample interaction in a desired region on the force distance curve. For contact mode scanning this region is the repulsive linear region on the curve.

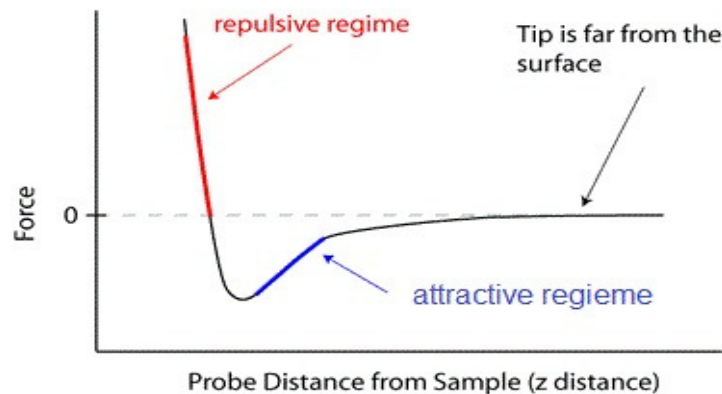


Figure 2.8: attractive and repulsive regions on the force-distance curve.

## 2.3 Electrical Construction

The electronics on the AFM provide power to its components, generate signals to drive its actuator and condition signals for analysis of the data. The block diagram in figure 2.9 shows the parts in this construction and each is then discussed in detail.

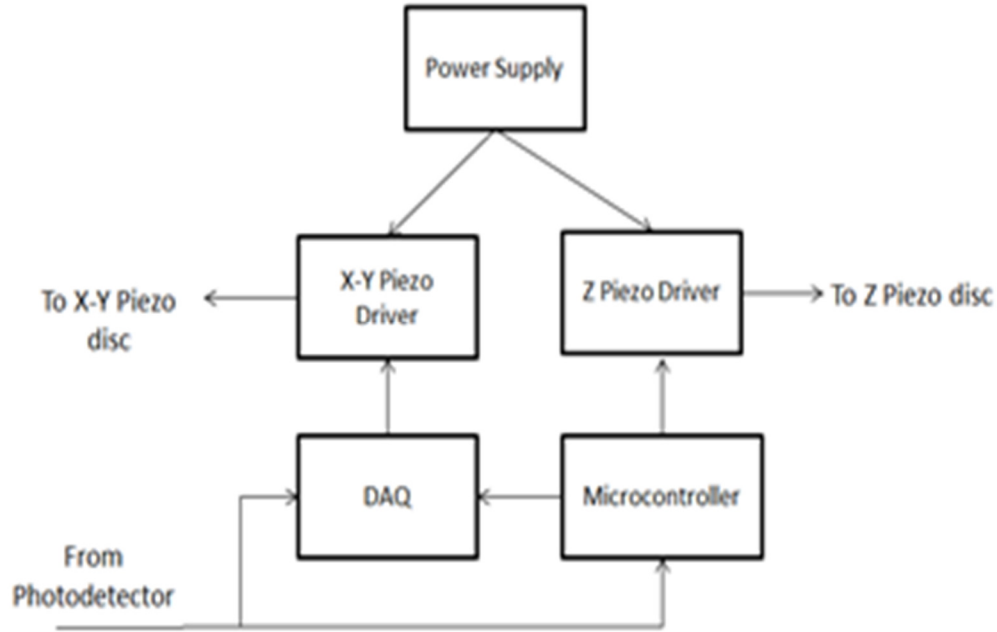


Figure 2.9: Electrical Construction Flow Diagram.

### 2.3.1 Power Supply

Piezoelectric materials require large driving voltages to operate. For this purpose a  $\pm 50\text{V}$  bipolar power supply is made. The power supply is standard in its construction with a step down transformer followed by a rectifier and filtering capacitors. This supply however is special in two ways. First the output of the rectifier is floating i.e. without reference to ground. This is essential to make this a bipolar supply. Secondly, Since the AFM output data is quite weak (in millivolts) and sensitive with important data in the second and third decimal place of the photodetector output; the power supply is regulated after the filtering stage to remove any ripples. For this purpose LM317 (positive voltage regulator) and LM 337 (negative voltage regulator) are used.

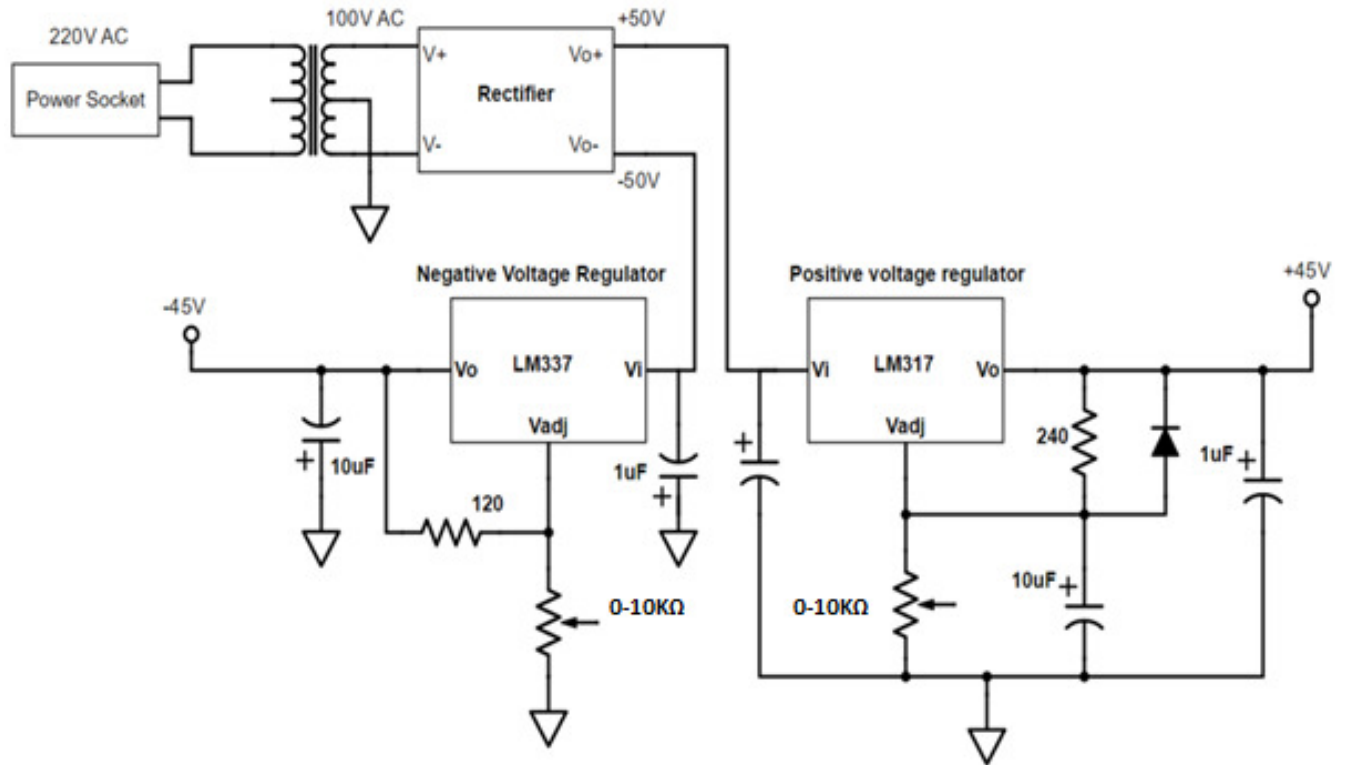


Figure 2.10: 100V bipolar power Supply.

### 2.3.2 X-Y axis Piezo Driver

The heart of the electronic design is the driver for the piezoelectric discs. To do a raster scan of a sample, triangular signals are used. Two such signals are generated from the DAQ board using the LabVIEW interface. One is a slow negative sloping linear signal that drives the Y axis slow scan. The other is a Triangular wave of a higher frequency that drives the fast X axis scan. Together these two signals create a raster scan pattern as shown in figure 2.11.

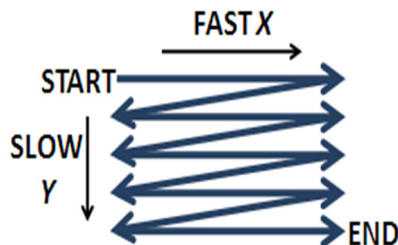


Figure 2.11: Raster scan pattern that drives the piezoelectric disc.

The electronics for the X and Y axis scan consist of two high voltage amplifiers (OPA445). These amplifiers pick the slow and fast scan signals and amplify them to 80V peak-to-peak (or  $\pm 40V$ ) triangular waves. These signals are then transferred to the four quadrants of the X-Y Piezo disc. The amplifiers are set in standard non-inverting configuration.

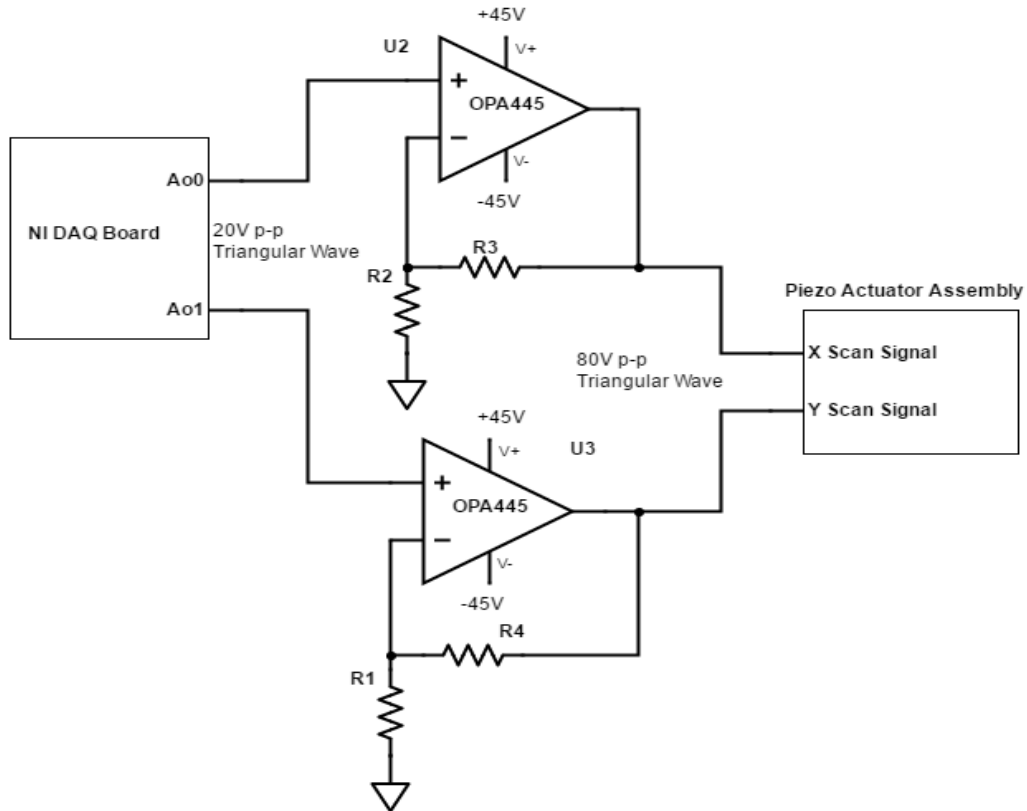


Figure 2.12: X-Y driving signal amplification circuit.

### 2.3.3 Z Axis Piezo Driver

This is different than the X-Y piezo driver because the driving signal comes from the microcontroller based on the feedback error. The microcontroller's DAC is connected to an OPA445 amplifier which turns the unipolar 0.55V-2.75V DAC signal to  $\pm 40V$  amplified bipolar voltage. The output pins are connected to the upper and lower side of the Z axis Piezo disc.



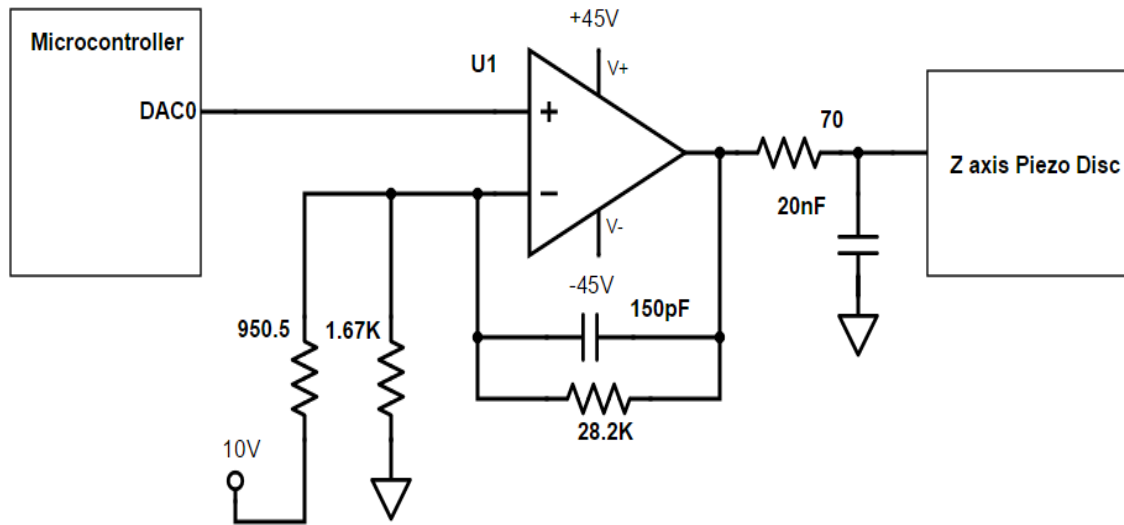


Figure 2.13: Z axis signal amplification circuit.

### 2.3.4 Signal Conditioning for Feedback

The output of the photodetector remains within a  $\pm 250\text{mV}$  range. This takes only a small part of the microcontroller's ADC range. To increase resolution it is desirable to amplify this signal. The signal also needs to be converted into a unipolar signal since the ADC cannot read negative voltages. To accomplish this, a two-stage amplifier circuit is constructed. The first stage consists of an ultra-low noise precision operational amplifier LT1028. This IC is specifically designed for amplifying low voltages. This IC's noise performance is extraordinary with only  $35\text{nV}$  peak-to-peak noise at  $10\text{Hz}$ . LT1028 amplifies the signal to  $\pm 3.3\text{V}$  without adding any noise and thus preserving the data.

The second part consists of an LTC2057 operational amplifier. This is also a low noise amplifier and converts the  $\pm 3.3\text{V}$  signal to a unipolar  $0\text{--}3.3\text{V}$  signal. The entire process could be done in one stage but giving offset requires providing a reference voltage which will always have some noise in millivolts destroying the original data. The two stage configurations gives necessary amplification and offset for the ADC of an Arduino Due board. The  $3.3\text{V}$  reference signal is picked up from Arduino board's own  $3.3\text{V}$  regulator output pin.

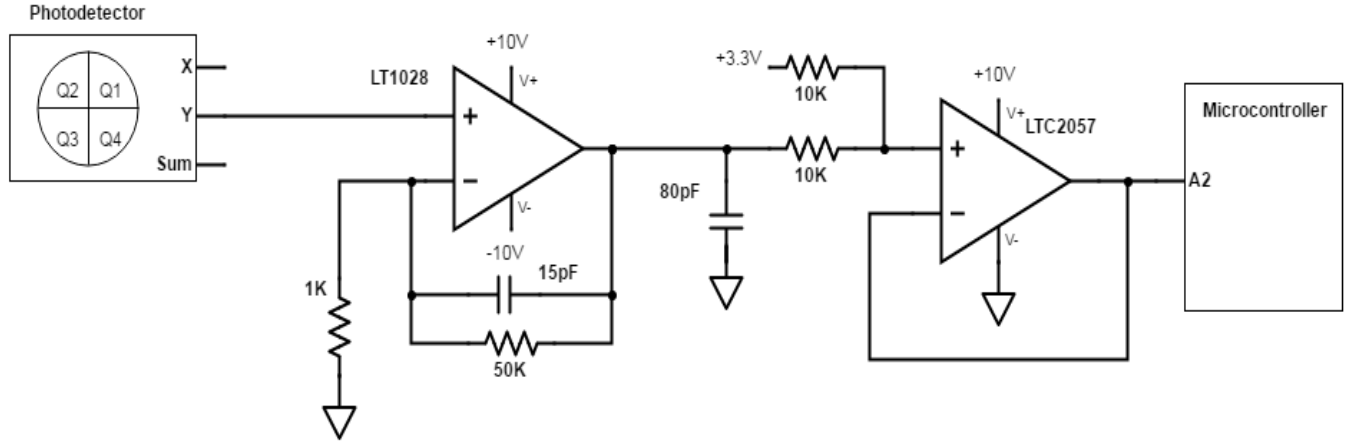


Figure 2.14: Signal conditioning circuit showing amplification and positive offset imparted to photodetector's  $Y_p$  signal.

## 2.4 AFM Operation

### 2.4.1 Generating X-Y Scan Signals

The X-Y piezo disc has to move in a raster scan pattern. Motion along X axis is slow and the disc sways from one end to another while the y axis motion is fast. The slow scan determines the total scan time and the fast scan determines the resolution and pixel pitch in the final image. Two triangular waves are generated for each scan axis. For a scan size of m-by-n microns, the x and y axis resolution in micrometers is given by:

$$R_x = \frac{2mf_{fast}}{f_s} \quad \dots\dots\dots (2.2)$$

$$R_y = \frac{nf_{slow}}{f_{fast}} \quad \dots\dots\dots (2.3)$$

Where  $f_{slow}$  and  $f_{fast}$  is the frequency of the slow and fast scan signals respectively and  $f_s$  is the sampling frequency of data acquisition. It is always desirable to have both resolutions equal to get pixels with an even pitch. This calculation is assuming a noiseless signal. However, the actual resolution is lower due to noise and the creep response of the piezo disc to driving signals.

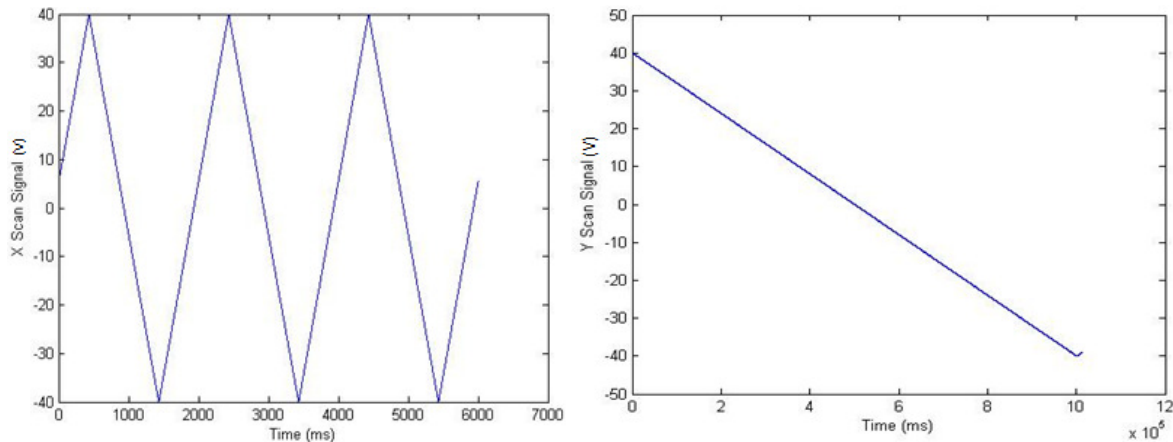


Figure 2.15: (a) X fast scan signal and (b) Y slow scan signal produced by DAQ.

The two triangular signals are generated by the NI DAQ analog output terminals with amplitude of 10V. The signals are then amplified by the OPA445 amplifiers discussed before to amplitude of 40V. These signals then drive the disc to few microns in both axes. The true scan area is determined by scanning a calibrated sample which will be discussed later.

## 2.4.2 Scanning Images

After testing signals for X Y and Z axis motion along with the photodetector's response, the AFM is in a position to scan samples. Preparing the AFM for a scan requires some steps which are now discussed.

- 1) **Powering On:** There are three power inputs for the AFM; one for the diode laser, one for the Picomotor and one to power up the electronics. All must be powered on and in stable state before the subsequent steps.
- 2) **Adjusting Photodetector Position:** The photodetector should be placed so that the laser spot hits its center and is not more than 9mm in diameter. To do this, the photodetector is moved first vertically and then horizontally to make sure both the  $X_p$  and  $Y_p$  signals are centered at 0V on the LabVIEW graphs.
- 3) **Engaging the tip:** The process of bringing the probe tip to the sample surface so we can scan images and measure forces is called “engaging.” The aim is to get the tip in close proximity so it is just barely coming into contact without bending. If the probe does not touch the surface, it is obviously useless, but if it's bent too much against the surface, it is equally useless. The tip is carefully brought near the surface, first turning the motor knob by hand, then very slowly with the Picomotor controls on the LabVIEW user interface. When contact is made, the Y axis signal steeps upward. At this point the motor is stopped and reversed very slowly to bring the cantilever to its original position so that there is no bending. Due to adhesive forces, the tip would remain in contact even if the motor is brought down further but that is not required.

- 4) **Generating X-Y actuating signals:** After contact is made, the two triangular signals are applied from NI DAQ board with calculated frequencies for a particular image size. For example a slow and a fast scan frequency of 0.005 Hz and 0.5 Hz at a sampling rate of 1 KHz will produce an image of size 1000x1000 in 1000 seconds with pixel pitch given by equations 2.2 and 2.3.

While engaging the tip, measuring the cantilever deflection gives the force distance curve. This curve lies in the core of AFM imaging and it is essential to know where the tip is on this curve. For contact mode scanning, the tip should be in the repulsive region which appears just after contact. This region is somewhat linear and a good signal swing can be obtained. Non-contact mode scanning uses the attractive region of the curve. This technique, although more advanced, provides less resolution and sensitivity than contact mode. A typical force distance curve obtained is shown in figure 2.16.

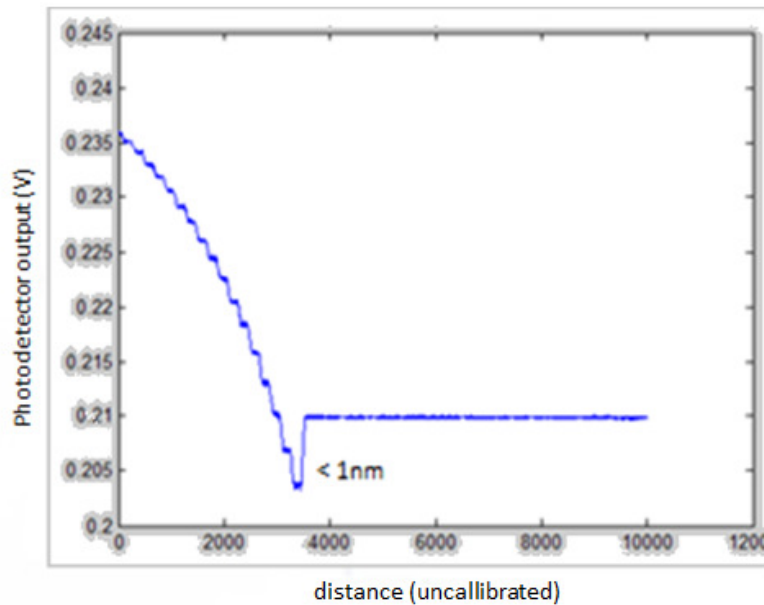


Figure 2.16: A typical force-distance curve.

Before a complete raster scan can be done, scanning a line on the sample provides good information about the piezo disc motion and detecting features on the sample's surface. In the line scan a bow-like motion is visible. This is due to the fact that the X-Y piezo disc does not move linearly but sways from left to right making a bow. This creates an artifact in the image.

Following the step by step procedure of image scan, we have obtained several images. The data comes sequentially in the form of a vector. Using Matlab, an image matrix is created by comparing X-Y piezo driving signal with the vector. The matrix is then converted into a grayscale image. This image is raw and contains numerous artifacts which obscure the true surface topology. Often nothing is visible at this stage. The raw image is passed through image processing algorithms. The steps with details are described in chapter 4 of this dissertation.

# Chapter 3

## Feedback Control of AFM

### 3.1 Motivation for Feedback Control in AFM Operation

The mechanics of AFM operation that have been discussed so far are termed as “Open Loop” i.e. a one-way process where a system is given an input and it generates an output purely depending upon its nature regardless of any constraint placed by the user. The data flow is in uni-direction as opposed to a feedback. The system in this case is the cantilever being deflected off the sample’s surface. The amount of deflection is not being monitored or controlled and the system is free to react to the stimulus. This is how all systems behave naturally when there is no constraint on their output.

Ideally an open loop mechanism is fine for the AFM to generate data however the reliability of this data can be an issue if the laser is not falling properly on the photodetector’s sensitive surface. The PDQ80A Quadrant detector has a circular surface of 12mm diameter. For samples with large height features, the laser goes off the surface. This limits the AFM to scanning small samples. The particular setup is capable to manage samples with features up to 500nm. In order to increase this range and get better results for large samples, a feedback mechanism is necessary which continuously monitors the output and provides feedback to the user which then can be used to adjust the assembly in real time so that the laser always shines within the detector’s photosensitive part. Feedback control enhances the results ordinarily obtained in open loop besides providing reliable operation [26].

### 3.2 AFM Feedback Loop

The feedback mechanism consists of the system that needs to be controlled, a sensor which is the quadrant photodetector and a controller which analyzes the difference between the output and the required response and calculates the necessary input that needs to be given to the system to get the desired response. The system in this case is a piezoelectric disc which moves up or down in nanometers based upon the voltage applied across its top and bottom surfaces. Figure 3.1 shows a typical response of the disc in open loop for different voltages.

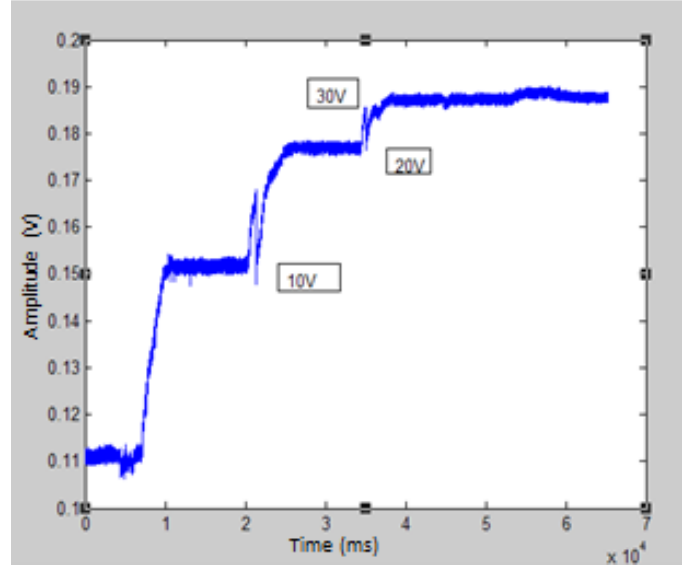


Figure 3.1: Response of Piezo disc to different voltages.

The controller being used is an Arduino Due board with a 32 bit ARM processor along with 12 bit ADCs and DACs. The processor runs at 84MHz which is more than what is needed. This is the only Arduino board which produces a pure DC output from two 12 bit DACs. All other boards generate a pulse width modulated signal when an analog output command is called. The control loop consists of the controller generated controlled output based on the feedback which is the y-axis ( $Y_p$ ) signal of the photodetector. The output then drives the sample up and down ensuring that at all time the laser stays at the same point on the detector's surface.

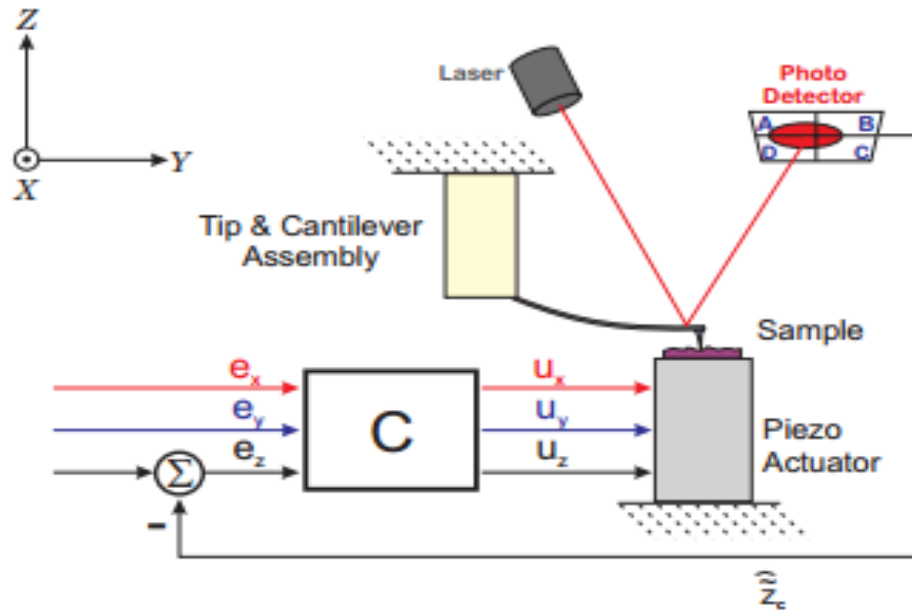


Figure 3.2: AFM feedback loop. Photo taken from [27].

A PID controller is the most common algorithm for feedback control. The theory and implementation of this algorithm are discussed here.

### 3.3 Fundamentals of PID control

A proportional-integral-derivative or PID controller is a control system that uses the difference of the output from a desired set point and calculates the necessary input to the system using the error, its derivative and integral over the past values. PID controllers have been hugely successful in all applications from industrial machinery to aircraft autopilot systems. The control equation for a PID controller is given by:

$$U(t) = K_p + K_i \int E(t)dt + K_d \frac{dE(t)}{dt} \quad \dots\dots\dots 3.1$$

Where  $K_p$  is the proportional gain,  $K_i$  is integral and  $K_d$  is derivative gain.

#### 3.3.1 Proportional Response

The proportional component depends only on the difference between the set point and the process variable. This difference is referred to as the error term denoted by  $E(t)$ . The proportional gain ( $K_p$ ) determines the ratio of output response to the error signal. For instance, if the error term has a magnitude of 10, a proportional gain of 5 would produce a proportional response of 50. In general, increasing the proportional gain will increase the speed of the control system response. However, if the proportional gain is too large, the process variable will begin to oscillate. If  $K_p$  is increased further, the oscillations will become larger and the system will become unstable and may even oscillate out of control.

#### 3.3.2 Integral Response

The integral component sums the error term over time. The result is that even a small error term will cause the integral component to increase slowly. The integral response will continually increase over time unless the error is zero, so the effect is to drive the steady-state error to zero. The steady-state error is the final difference between the process variable and set point. A phenomenon called integral windup results when integral action saturates a controller without the controller driving the error signal toward zero.

#### 3.3.3 Derivative Response

The derivative component causes the output to decrease if the process variable is increasing rapidly. The derivative response is proportional to the rate of change of the process variable. Increasing the derivative gain ( $K_d$ ) parameter will cause the control system to react more strongly to changes in the error term and will increase the speed of the overall control system response. Most practical control systems use very small derivative gain ( $K_d$ ), because the derivative response is highly sensitive to noise in the process variable signal. If the sensor feedback signal

is noisy or if the control loop rate is too slow, the derivative response can make the control system unstable.

### 3.4 Controller Tuning

The process of setting the optimal gains ( $K_p$ ,  $K_i$  and  $K_d$ ) to get an ideal response from a control system is called tuning. There are different methods of tuning of which the “guess and check” method and the Ziegler Nichols method will be discussed. The gains of a PID controller can be obtained by trial and error method. In this method, the I and D terms are set to zero first and the proportional gain is increased until the output of the loop oscillates. As one increases the proportional gain, the system becomes faster, but care must be taken not make the system unstable. Once P has been set to obtain a desired fast response, the integral term is increased to stop the oscillations. The integral term reduces the steady state error, but increases overshoot. Some amount of overshoot is always necessary for a fast system so that it could respond to changes immediately. The integral term is tweaked to achieve a minimal steady state error. Once the P and I have been set to get the desired fast control system with minimal steady state error, the derivative term is increased until the loop is acceptably quick to its set point. Increasing derivative term decreases overshoot and yields higher gain with stability but would cause the system to be highly sensitive to noise.

#### 3.4.1 Zeigler Nichols Method

The engineering team of Ziegler and Nichols developed this method in the early 1940's. It is a heuristic tuning method that gives extremely good values for controller gains by achieving “quarter wave decay” which is a condition where the amplitude of oscillation drops to one-fourth of its value in the previous cycle after a disturbance is recorded.

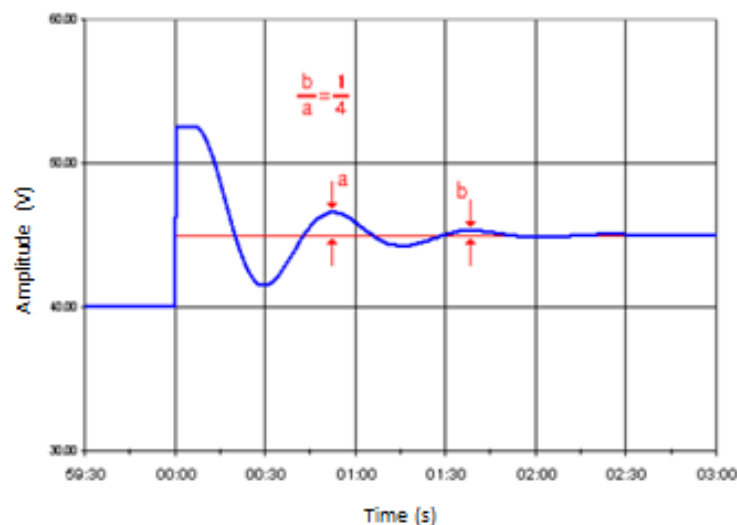


Figure 3.3: Quarter wave decay condition exemplified.



To achieve quarter wave decay, Zeigler came up with the following method

- 1) Initially keep  $K_i$  and  $K_d$  at zero and start increasing  $K_p$  form zero. The response will start to take shape.
- 2) Increase  $K_p$  until the response of the system becomes oscillatory and the output has a steady sinusoidal response. This value of proportional gain is called the critical gain  $K_c$ . Note time period  $P_c$  of the oscillation and  $K_c$ .
- 3) Use the table below to calculate all the parameters of the controller

Control Mode	$K_c$	$T_i$	$T_d$
P	$0.5K_u$	---	---
PI	$0.45K_u$	$P_c/1.2$	---
PID	$0.6K_u$	$P_c/2$	$P_c/8$

Table 3.1: Formulae for Zeigler Nicholes method.

Finally, the controller gains are given by these relations:

$$K_p = K_c \quad K_i = \frac{K_c}{T_i} \quad K_d = \frac{K_c}{T_d} \quad \dots\dots\dots 3.2$$

### 3.4.2 Tuning Controller Gains for the AFM

This method was employed for the AFM to tune the controller parameters. Before designing the controller, it is very important to observe the system's step response to see the stability of the system. This helps in determining what kind of controller (P, PI, PID PII) will be needed. Figure 3.4 shows the step response of the Z axis piezoelectric disc. A square wave signal with amplitude of 20V was applied across its top and bottom electrode.

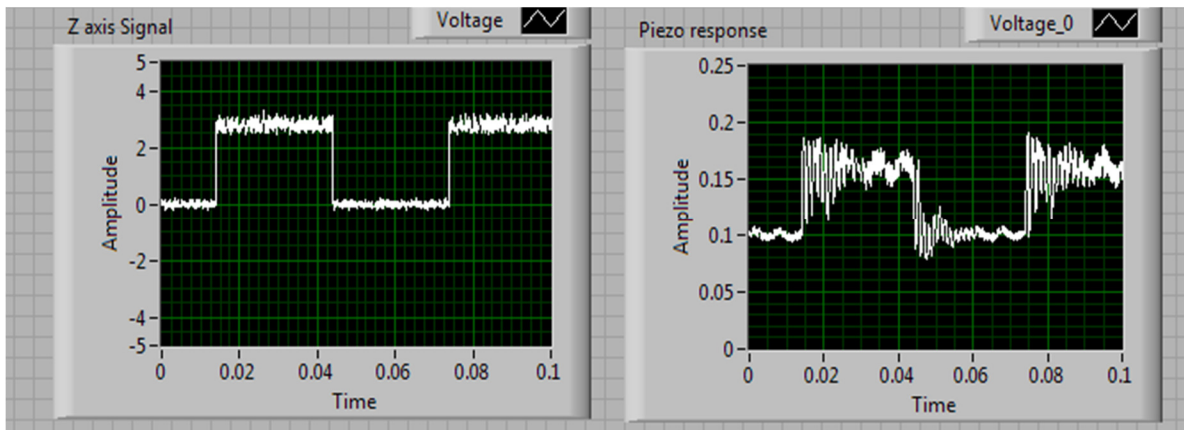


Figure 3.4: Step Response of Piezoelectric Disc with (a) showing 25V square wave as input and (b) tis output.

Some conclusions can be drawn from the response

- The system is stable with an under-damped response
- The transient of the piezoelectric disc takes a relatively longer time for the AFM operation
- The response is noisy so there will be some noise in the control loop. The derivative term cannot be used in the controller so  $K_d$  must be zero.

Now that it has been established that a PI controller will suit the AFM, the Zeigler Nichols method can be followed to obtain the values for  $K_p$  and  $K_i$ . The critical gain condition is shown in figure 3.5.

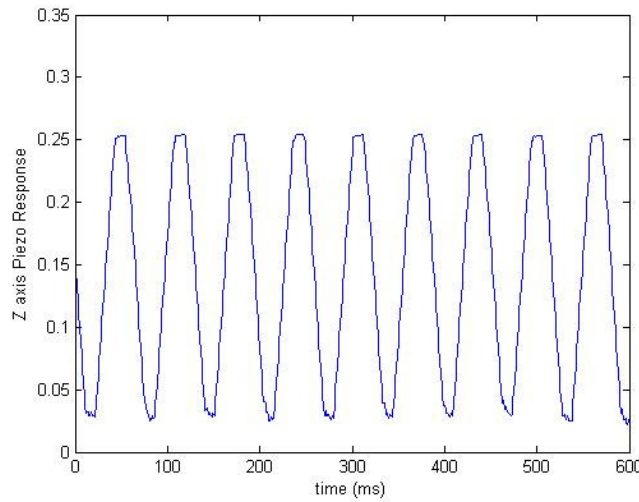


Figure 3.5: System Response at Critical Gain  $K_c$

This condition is obtained at a critical gain  $K_c = 0.49$ . The corresponding  $T_c$  is 65 ms. Using table 3.1, the corresponding values of all the control gains come out to be:

$$K_p = 0.3 \quad K_i = 10.9 \quad K_d = 0$$

## 3.5 Performance of AFM with PID control

### 3.5.1 Response to set point adjustments

The piezoelectric disc is tuned to the calculated gains and produces good response with negligible steady state error and fast transient time. The response to changing reference is shown below

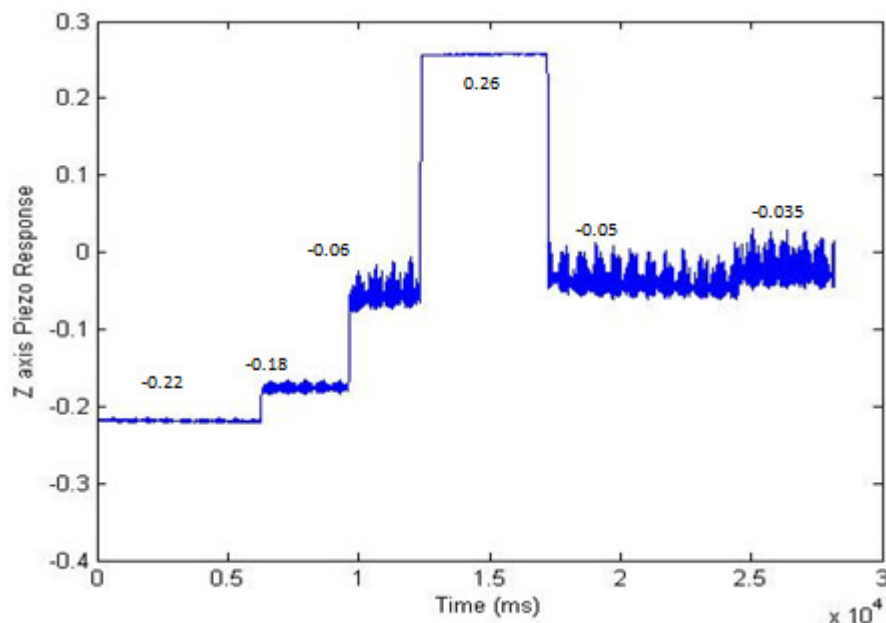


Figure 3.6: Response to changing Set Point.

### 3.5.2 Response to Disturbances

The AFM must also be able to cancel effects of external disturbances. During the operation, the piezoelectric disc has the job to maintain the cantilever at a fixed point and overcome the disturbances caused by changes in surface topology of the sample being scanned. Typically, a PID controller can overcome disturbances up to the second order functions. In the case of the AFM disturbances are usually either steps or ramps for which the controller is capable of cancelling. Figure below shows the “Bow motion” of the X-Y axis piezoelectric disc being cancelled by the controller.

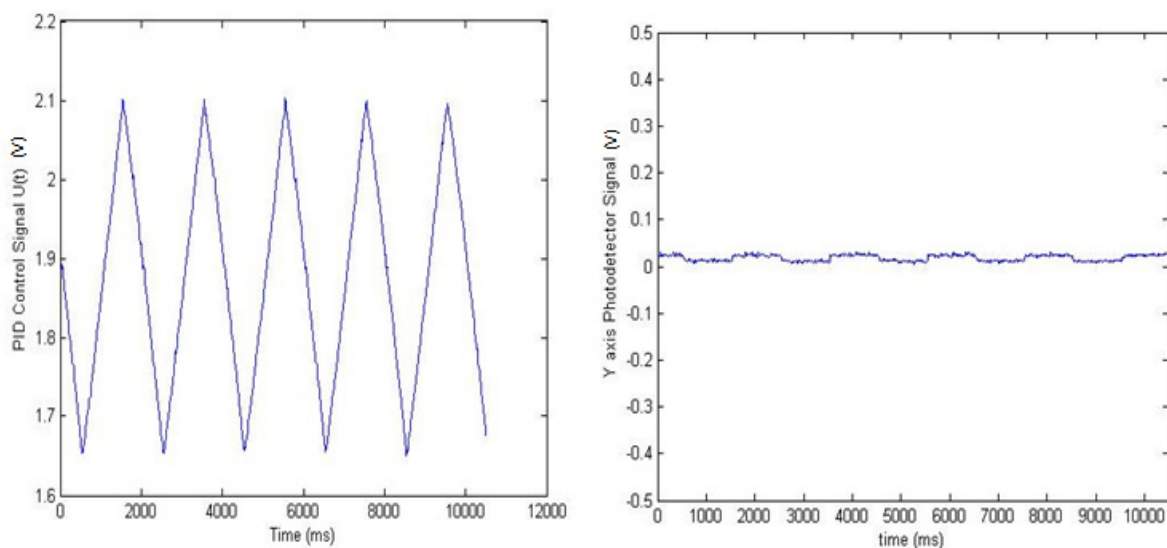


Figure 3.7: Cancellation of the “Bow motion” by the PID Controller.

When the AFM is running in closed loop, the data is no longer provided by the photodetector. Instead, the data is obtained in the form of an “error image” by the output of the PID controller after processing the feedback error. The images obtained in this way have a reversed topology, i.e. the mountains become valleys and vice versa. The results obtained with control of images with large height differentials are superior to what were obtained without control. Below is a comparison of a sample with valleys of height difference equal to 500nm. Without control, the laser falls out of the detectors surface while scanning the valleys and topography obtained is incorrect.

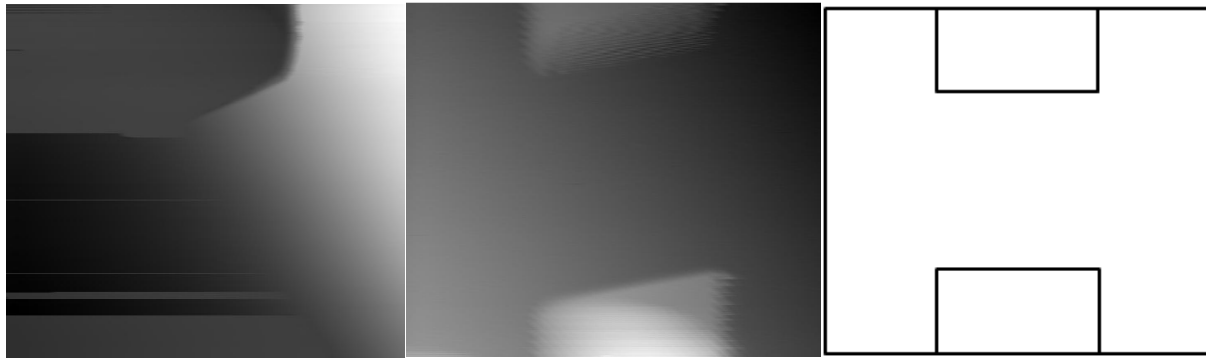


Figure 3.8: Image of two 500nm pillars (a) without Control, (b) with control and (c) actual topology.

### 3.5.3 Sampling Rate, Bandwidth and Noise Considerations

Since the controller is designed on a noisy feedback loop, the bandwidth of the loop and the clock frequency of the microcontroller become important. Figure 3.8 (a) shows a piece of y-axis signal obtained at a **sampling rate of 50 kHz**. The frequency analysis of this signal reveals noise components at higher frequencies. Note that the only useful data is present at DC (0 Hz). This is problematic since the frequency sweep of the piezoelectric disc reveals that it has high amplitude in the 600-1000 Hz range (figure 3.8 (b)). The Arduino Due board runs a typical PID controller code at 200-400 KHz which creates enough bandwidth to allow noise in this range. The disc will not settle at any point since a small component of photodetector’s noise is driving it at resonance. This problem becomes clear when the code is executed. The piezo disc produces a sound due to vibrations at resonance and is unable to settle at the given set point (figure 3.9).

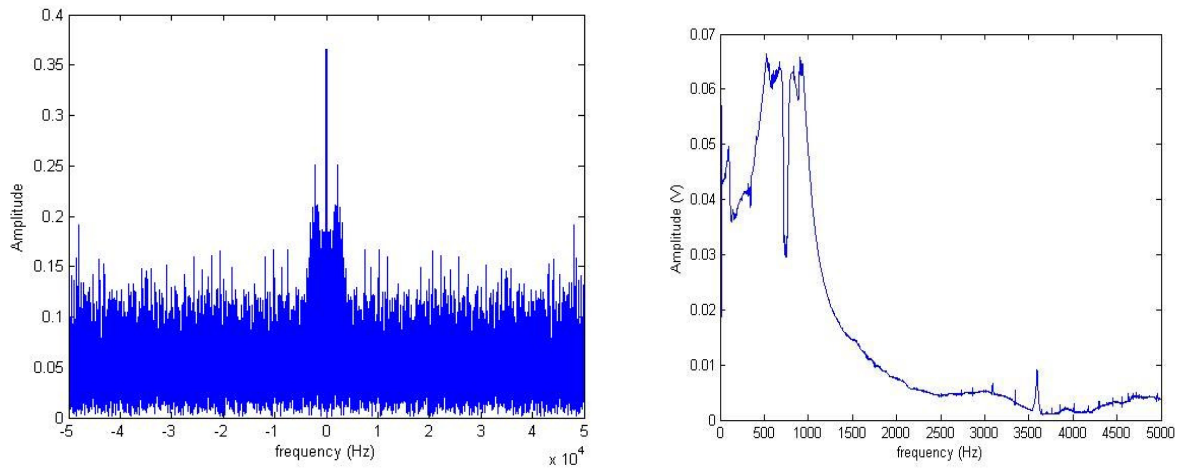


Figure 3.8: (a) frequency response of photodetector's signal (b) Frequency Sweep of Piezoelectric disc.

Figure 3.9 demonstrates the problem of noise with a plot of the controlled output of the piezoelectric disc. Notice when the set point is close to zero the disc doesn't settle but vibrates with a mean equal to the set point. The problem is particularly visible near zero because the DC part of the signal is very small and the response due to noise at higher frequencies dominates the output.

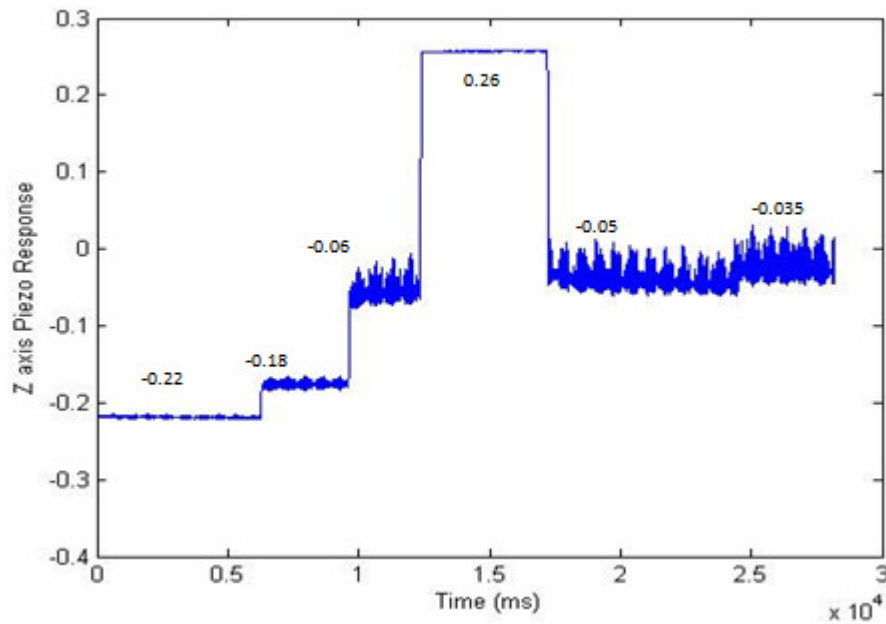


Figure 3.9: Response of piezo disc for varying set points with control.

# Chapter 4

## AFM Imaging

### 4.1 Acquiring Images

The AFM generates data that determines x and y axis displacement of the cantilever at the set sampling rate of the data acquisition device. The data obtained this way is sequential and needs to be sorted out. Some of the processing is done in real time while the scan is running and remaining is done post-scan. Following are the steps taken to generate a raw AFM image

- Real time processing AFM data to remove noise and smoothen the signal
- Storing data for post-processing
- Sorting the sequential data into images

#### 4.1.1 Noise Removal and Smoothening of signal

Before any enhancement can be made it is essential to find all the sources of noise present in the system and their bandwidth so that they can be adequately filtered.

##### 4.1.1.1 Sources of Noise in AFM

The noise in AFM data mainly comes from these sources:

- **Shot noise:** Most of the noise in the AFM data is shot noise of the Quadrant Photodetector. This noise is due to randomness in the quantity of incoming photons in the laser beam as well as randomness in generation of electrons in the semiconductor material of the detector. This noise lies at high frequencies
- **Johnson noise:** This is a relatively small noise caused due to the trans-impedance amplifiers in the Photodetector. Some of this noise comes from the X Y and Z axis amplifiers and signal conditioning electronics.
- **Mechanical vibrations:** This part is negligible unless there is some activity in the vicinity of the AFM. The apparatus is highly sensitive even to very small vibrations including loud noises.

##### 4.1.1.2 Noise Removal

Basic noise removal is done in real time by filtering the incoming data on the LabVIEW interface. A moving average filter with a history of 20 samples is applied which acts as a low pass filter and removes high frequency noise thus smoothening out the signal.

$$y[i] = \frac{1}{M} \sum_{j=0}^{M-1} x[i + j] \quad \dots\dots\dots 4.1$$

This filter is enough to overcome the high frequency noise in the data and reveal true variations in the signal. It is important to note that the sampling rate here is 1 KHz and the noise bandwidth is 500 Hz (half of sampling frequency) for which a 20 sample moving average filter works well.

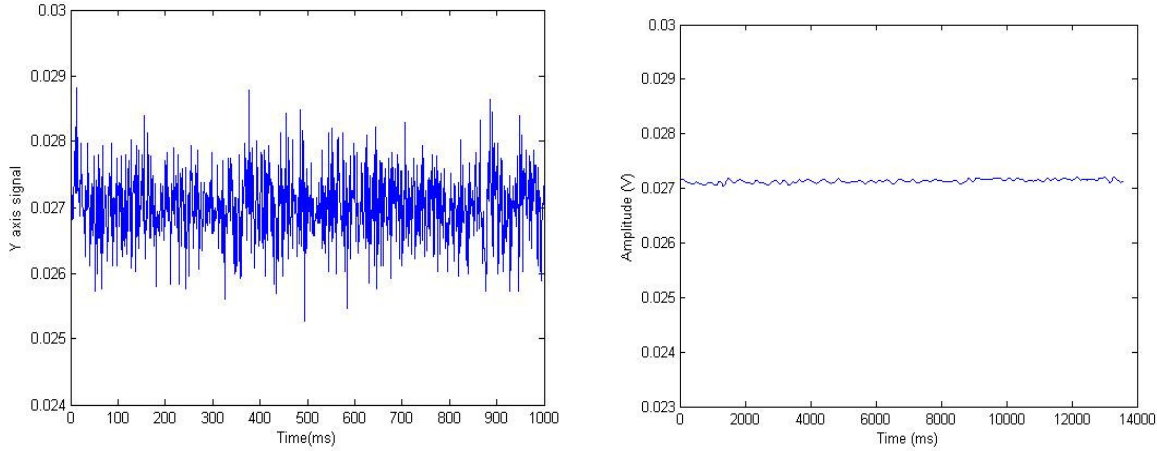


Figure 4.1: Photodetector signal (a) before filtering (b) after filtering.

#### 4.1.2 Sorting Data into Images

After the signal is filtered, it is sorted into a Matrix. Matlab is used for this task. The sequential vector containing the data is placed in successive rows of a matrix by correlating it with the fast scan driving signal. Every other row is flipped since the cantilever moves back and forth while scanning in the fast axis. After this the matrix is converted into a grayscale image with the maximum value being assigned white color and the minimum being assigned black. So the raw image shows the sample's surface topography in the form of a grayscale. Features high in z axis appear brighter than the lower ones. This image does not necessarily show a clear topography. In fact small images of small features usually appear flat and featureless as the real information is concealed within the large variations in data due to many image artifacts which are discussed later in this chapter. To remove these unavoidable artifacts, image processing is necessary.

## 4.2 Processing AFM Images

Processing of any SPM data is done in these steps:

- Baseline correction and leveling
- Removing grains, scan strokes, abrupt maxima and minima (impulse noise)
- Image histogram specification and assigning color to data
- Frequency domain filtering (Smoothing, sharpening, mean, median etc.)

### 4.2.1 Baseline Correction

This is the most important and sometimes the only image processing step taken for the AFM data. The motion of the piezoelectric discs is not linear and they move in a bowl-like manner which creates successive ups and downs in the image. These variations cover the entire color scale and hide the surface topology. In addition, the sample and the optical bench are not perfectly horizontal and a tilt of even a few seconds of an arc creates rising and falling topology at the nanometer scale. This is solved by fitting a curve to individual rows of the data. Typically a first or second order polynomial is fitted and subtracted from the data. This corrects the baseline of the image. The sample features become visible at this step.

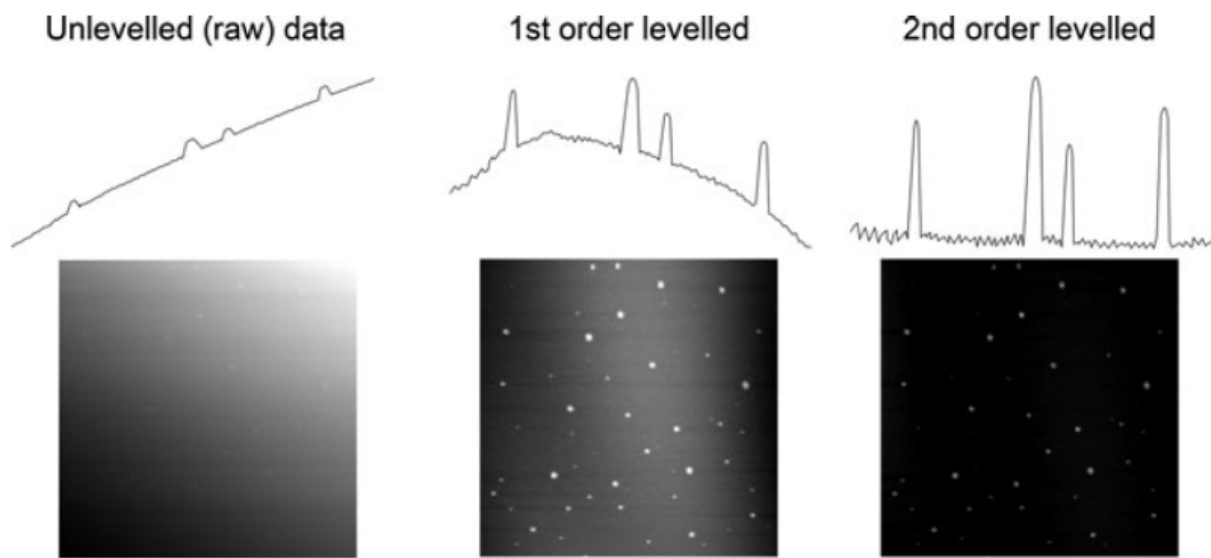


Figure 4.2: Leveling AFM data to correct baseline. Image taken from [28]

### 4.2.2 Removing outliers, scan strokes and correcting scan lines

This is done by leveling outliers that appear in small patches usually in rectangles. This artifact is caused due to the tip being dragged at some point in the scan. Other outliers and abrupt slopes are also removed as they don't represent any useful data. This step also removes artifacts in the form of dark granular structures.

The AFM image rows sometimes get misaligned. This is removed by an algorithm that matches height median over the image and corrects any such misalignment. All of this is done by a specialized SPM analysis software called "Gwyddion".



### 4.2.3 Image Histogram Specification

Usually the topography occupies a small part of the color range because of small variations in the signal. This can be adjusted by specifying the maxima and minima of the data or by equalizing the histogram of the image. Histogram Equalization assigns gray levels to images based on their probability of occurrence in the image. So the topography is assigned a wider range of colors which makes it clear for viewing. The image is also assigned a color scheme.

### 4.2.4 Frequency domain filtering

This step is optional and may not be needed. AFM images sometimes appear blurred or have sudden variations or may contain noise. These images can be enhanced and cleaned with image filters. A mean or median filter removes high frequency noise and impulse noise in the data. A Laplacian filter sharpens the edges making the topology more crisp and clear. All these filters, however, also have degrading effect on the image data. Smoothing the image may blur details and sharpening the image will also enhance noise components in the image. So this step is usually done by trial and error and multiple filters are applied to observe which function best.

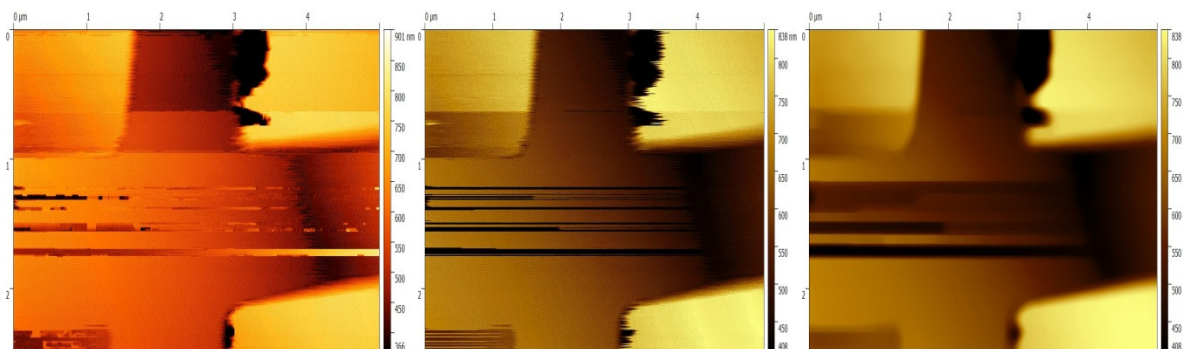


Figure 4.2: Image filtering (a) original (b) median filtered (c) low pass filtered acquired on a silicon sample with 500 nm SiO<sub>2</sub> pillars.

## 4.3 Image Artifacts

### 4.3.1 Probe Artifacts

#### 4.3.1.1 Blunt Probe

Typically, blunt probes will lead to images with features larger than expected, with a flattened profile, due to the effect shown in figure 4.3. Note that holes in a flat surface will show the opposite effect, appearing smaller with blunt probes than with sharp ones.

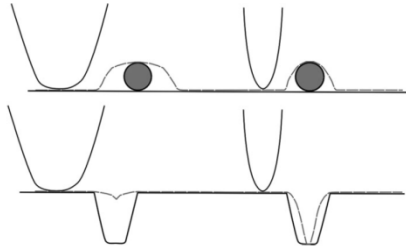


Figure 4.3: Effect of sharp and blunt probe.

#### 4.3.1.2 Contaminated or Broken Probes

Contamination of AFM probes is quite common, and scanning certain samples leads to dirty probes more quickly than others. In particular, biological or other soft samples, or any sample with loose material at the surface, tending to contaminate probe tips quickly, and ultimately leading to image degradation [30].

#### 4.3.1.3 Probe Sample Angle

When scanning large features, artifacts can be introduced by having a large angle between the probe and the sample, as illustrated in Figure 4.4. This problem is solved by adjusting the angle between the probe and the sample so that they are perpendicular.

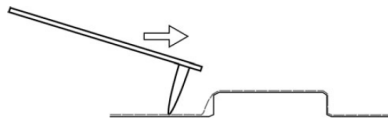


Figure 4.4 Angled probe

### 4.3.2 Piezoelectric Scanner Artifacts

#### 4.3.2.1 Scanner Bow

The piezoelectric disc used as a scanner moves in a slightly curved motion making a bow creating a false contour on the resulting images. This appears as slightly bright background at the center and darker at the edges. This artifact cannot be removed in the hardware. It is removed by correcting the baseline in the software as discussed in section 4.2.1.

#### 4.3.2.2 Piezo Hysteresis and Creep

Creep in piezoelectric discs gives rise to the phenomenon that when an instantaneous voltage is applied to the piezoelectric and maintained, the response of the material does not follow exactly the applied voltage, but instead continues to move in the same direction as the initial offset, even when the voltage is no longer changing. This leads to overshoots over edges and an effect called “Scanner Drift” shown in figure 4.6.

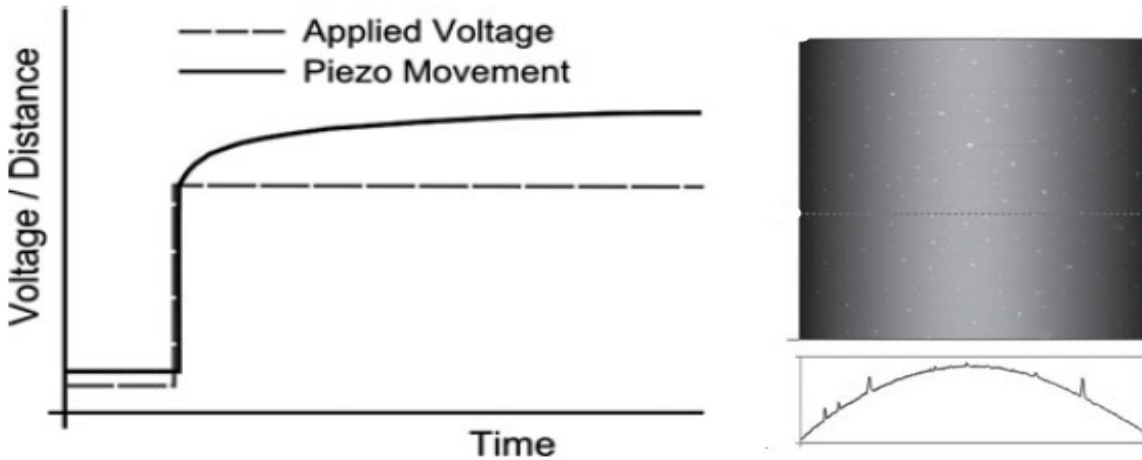


Figure 4.6: (a) Piezo creep (b) bow of Piezo scanner. Figure taken from [28].

#### 4.3.3 Other Artifacts

##### 4.3.3.1 Leveling Artifacts

Leveling changes the entire AFM image, so the resulting image is different from the raw data. However, it is very often a necessary procedure before useful information can be extracted from an image. Commonly, leveling artifacts are introduced by polynomial fitting routines. This can be avoided by leveling parts of the image.

##### 4.3.3.2 Laser Interference Pattern

This is one of the most common artifact in AFM images. It shows up as strips of bright and dark regions over the entire image. This happens when the laser is not properly focused and aligned on the cantilever and another reflection from somewhere else also falls on the detector and interferes with the reflection off the cantilever to produce an interference pattern. This artifact can be overcome by a better alignment of the laser. Using a low coherence light source can also help.

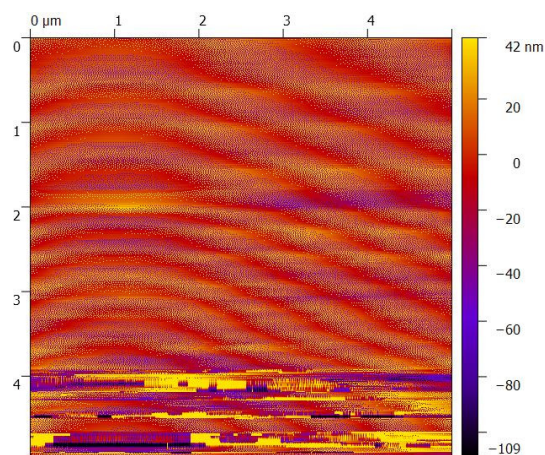


Figure 4.7: Laser interference pattern visible in generated image.

#### 4.3.3.3 Vibrations

Vibrations in the vicinity due to other machinery, sound or vibrations of the building can cause periodic patterns in the image. This can be avoided by isolating the AFM apparatus from loud noise and damping the table on which it is placed to cancel floor vibrations.

The AFM has been setup on an optical bench which dampens mechanical vibrations with springs present inside screw holes. The optical assembly is covered from all sides to isolate from air drafts, light and sound.

### 4.4 Actual Images

The very first image we scanned was of a calibration sample having 500 nm  $\text{SiO}_2$  pillars on a Si substrate (figure 4.8). Figure 4.9 shows the results of the scan. The scanner was able to pick up two pillars which can be seen in yellow color against brown background. This image, although very clear has scratches in it specially near the border of the pillars. This indicates that the contact was strong and the tip had dragged over the sample's surface.

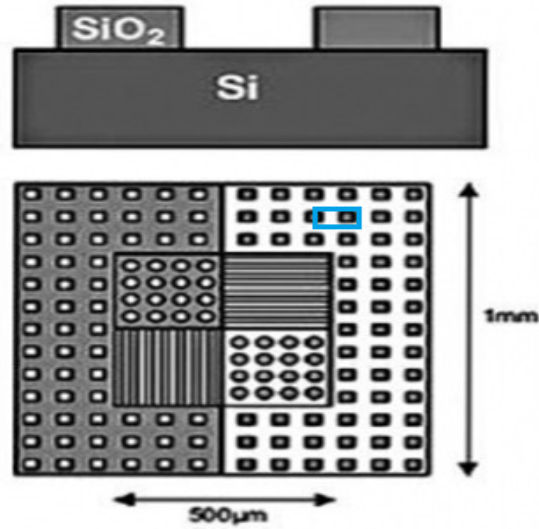


Figure 4.8: 500 nm calibration sample with scan region marked in blue (HS500MG manufactured by Tedpella).

The image processing steps involved were

- Baseline correction: figure 4.9 (a) shows the slanted base of the scan which was corrected to get correct features.
- Histogram equalization: more color range was provided to the pillars and the background. This was necessary since there were patches of outliers (colored black) which were not part of the topology and needed to be suppressed.
- Some scan strokes were removed using Gwyddion's algorithms to make the image more clear.

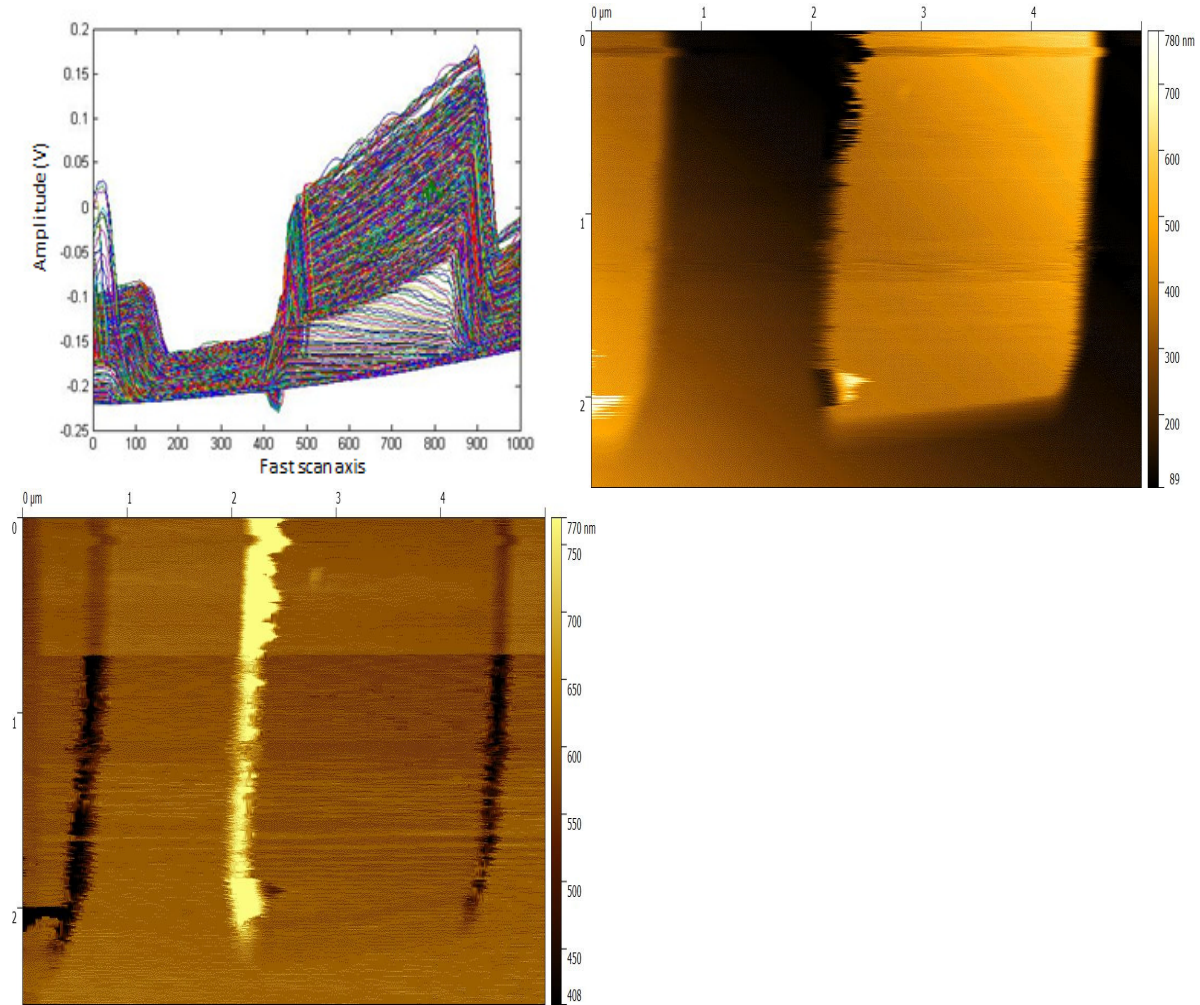


Figure 4.9: (a) Raw line scans, (b) Y axis image and (c) X axis image of a 500 nm calibration sample.

Features of smaller size were also scanned. Figure 4.10 shows scan of 500nm square grooves in a silicon substrate. A similar sequence of image processing steps as discussed for the previous image were used. It is important to note that this image, like the other, has black patches at the edges of the groove. This happens when the laser goes off the detector's surface when the cantilever is climbing up a step because the tip bends in tip's reflecting surface bends away from the step as the tip climbs up. Notice that the boundary where the tip falls down does not have such black patches.



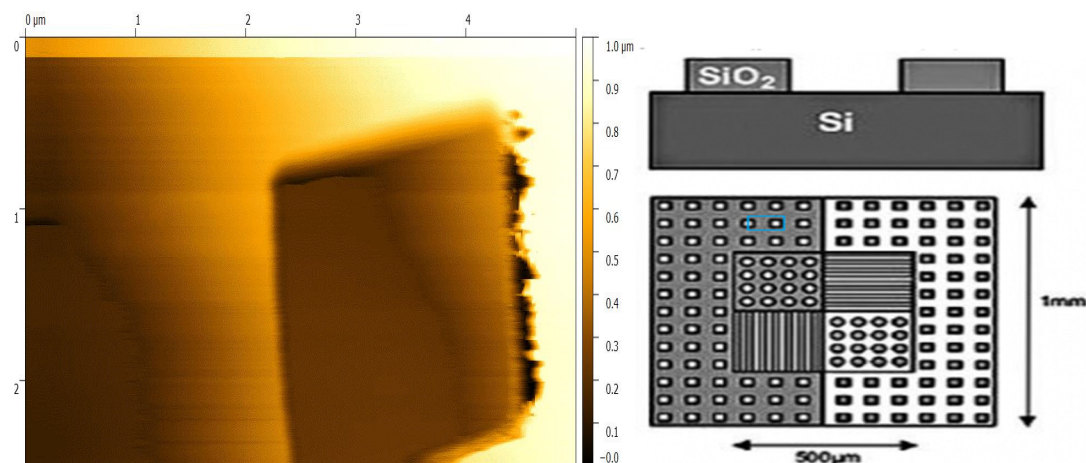


Figure 4.10: (a) Scan of 500 nm grooves in a calibration sample and (b) sample topology with a can region marked with blue.

The problem at the edges is resolved by imaging such step heights in feedback control. Figure 4.11 shows the image of 100 nm square grooves imaged in feedback. There are no dark patches or scan strokes near the edges. Notice also that the topology is reversed i.e. the grooves appear to be pillars. This is because the PID controller attempts to cancel the cantilever motion due to changes in surface features and so creates an error image which has an inverted topography.

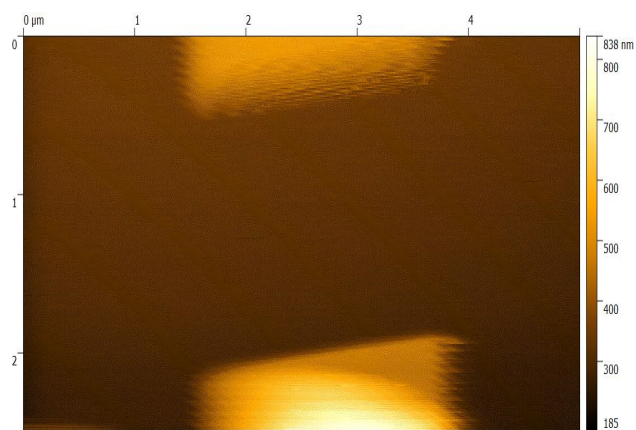


Figure 4.11: 100nm grooves scanned in feedback control.

One of the most challenging samples to scan was a 30nm cellulose acetate grid shown in figure 4.12. The sample has periodic 30 nm deep valleys in both axes.

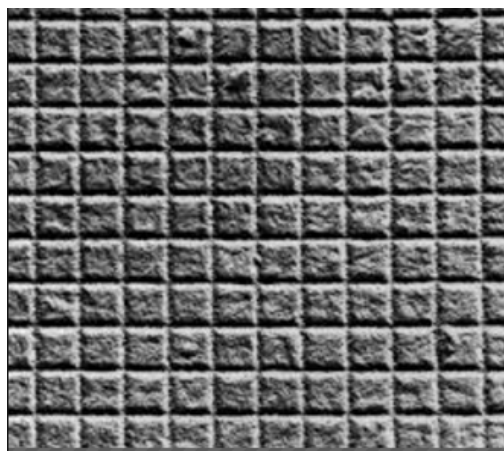


Figure 4.12: Topography of 30 nm cellulose acetate grid (model no: 607-AFM manufactured by Tedpella).

Imaging this sample gives a unique opportunity to elaborate on challenges in AFM imaging that is to extract a weak topographical signal masqueraded by artifacts. Consider figure 4.13:

- Initially the data is translated into a grayscale image and there is no feature visible. The slanting baseline and a diagonally aligned bow is visible. These are scanner artifacts. (figure 4.13 (a))
- Figure 4.13 (b) shows the image after subtracting a third order polynomial background from the data. The uneven surface becomes flat
- Then the histogram is adjusted in such a way that maximum amount of color range is given to the small variations that represent the actual topography. At this point a grid pattern becomes visible as shown in figure 4.13 (c)
- Since the variations in topography are of the order of molecules, the cantilever can only scan that part of the sample at which the force distance curve allows maximum variation of force per unit change in distance. Since the Piezo scanner is not linear as discussed in section 2.2.3, this happens for a part of the image. That part is then cropped (figure 4.13 (d)) and further processed
- The final image is obtained after passing the image through frequency filters. In the present image (figure 4.13 (e)), a high pass filter has been applied with a window size adjusted by hit-and-trial. For the current image the filter used a 5x5 laplacian window.



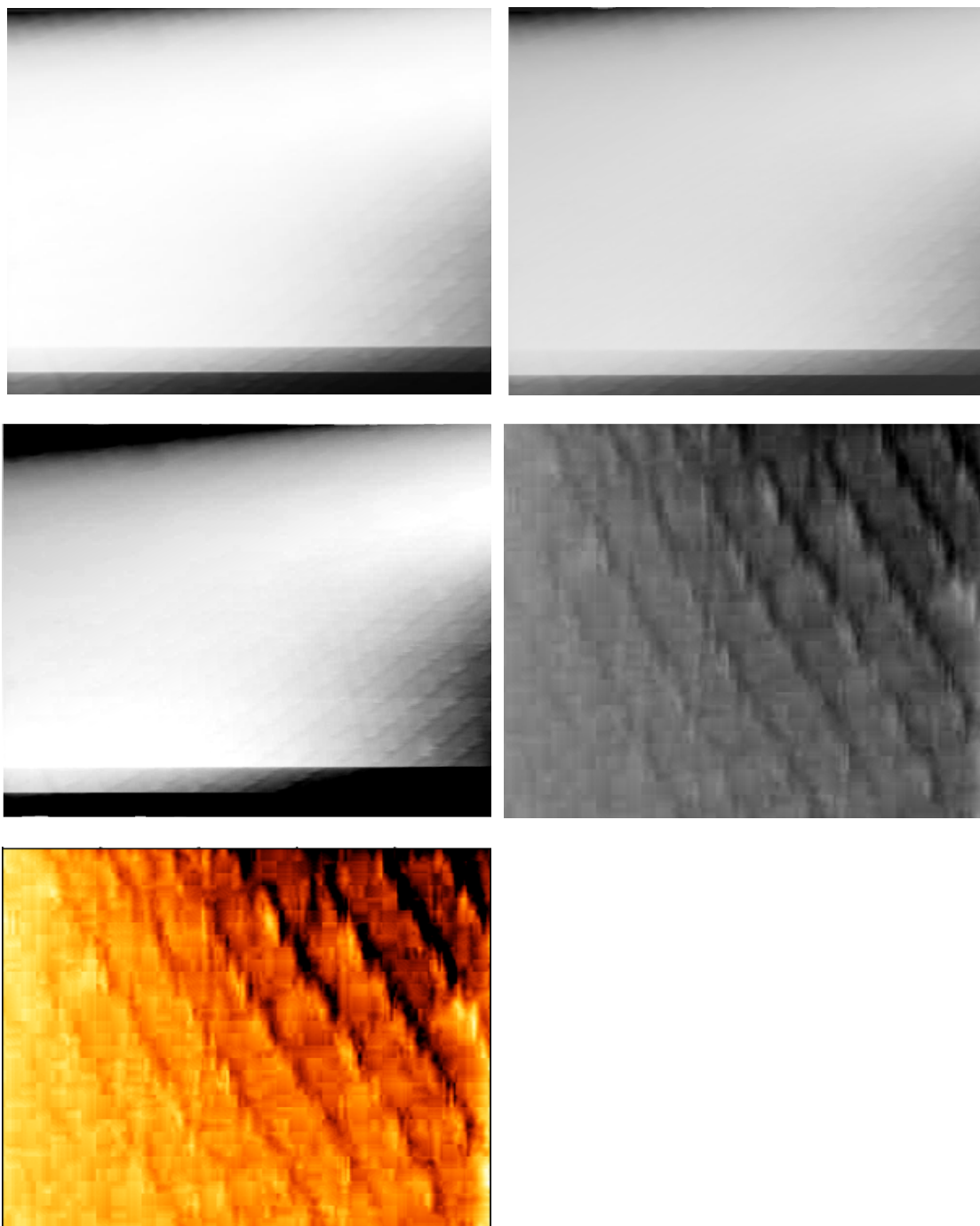


Figure 4.13: Steps in AFM image processing.

This sample is of high interest since it lies close of what the AFM is presently capable of resolving. So this sample was imaged again with four times slower speed. The scan took 66 minutes and created a 2000x2000 pixel image. The result was significantly better than the one in figure 4.13 (e). The grid lines are more clear especially in the direction of fast scan that the previous image fails to clarify. Figure 4.14 shows this scan result.

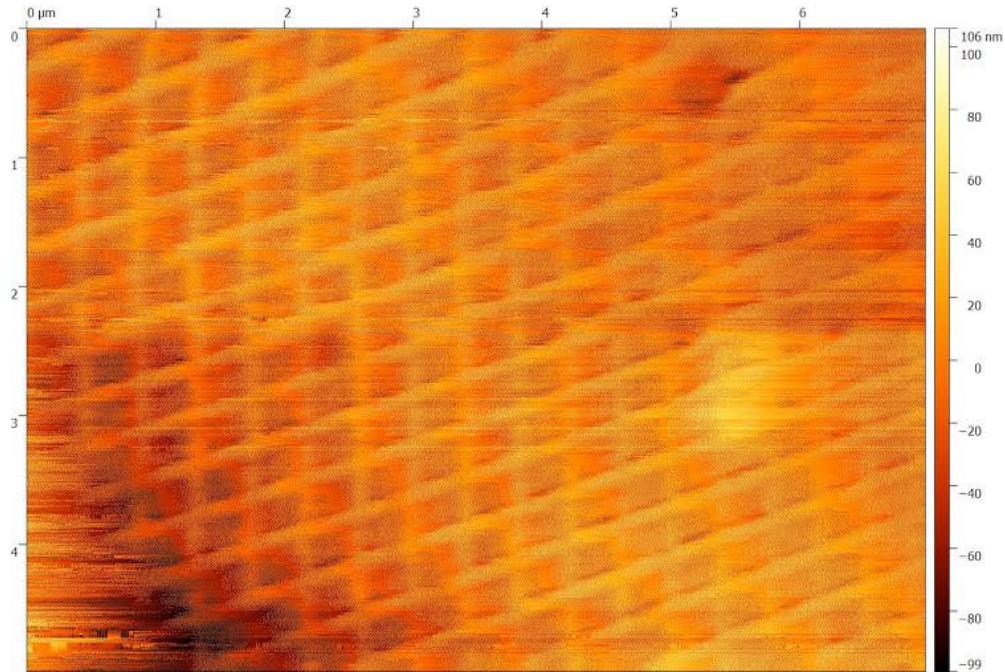


Figure 4.14: 30 nm cellulose acetate grid scanned at a slower rate.

## 4.5 Further Improvements and Future Directions

### 4.5.1 Automated Tip Engagement

Commercial AFMs have an automatic process which engages the tip to the sample. This construction requires a user to perform this task manually by observing the y axis signal of the photodetector. Another addition would be augmenting the automatic engagement process to adjusting level of contact of the tip. This will require the microcontroller to communicate with the picomotor while the tip is being engaged to set the reference value.

### 4.5.2 Real Time Image enhancement and Processing

Most of the AFM image processing is done after the scan is done and the raw data is saved in memory. A more robust way would be to have all the image processing steps to be done either in real time while the scan is running or just after scan is complete by algorithms the require minimal user inputs. An FPGA will be very suitable for this task due to its high clock speed and ability to optimize digital algorithms to run at maximum speed.

### 4.5.3 Improved laser focusing and alignment

The laser spot is larger in size than the reflecting surface of the cantilever. Improvements can be made by using lenses with much sharper focusing ability and expanding the laser beam before focusing it.

#### **4.5.4 MFM, EFM and the likes**

This AFM project has set the base for any variant of SPM to be easily created by simply loading the appropriate probe. All the data acquisition, processing and analysis tools have been designed and interfaced with the hardware. This project will be able to provide scientists of interdisciplinary interests to take measurements of many physical properties including friction and surface properties, thermal properties, magnetic coefficients etc.

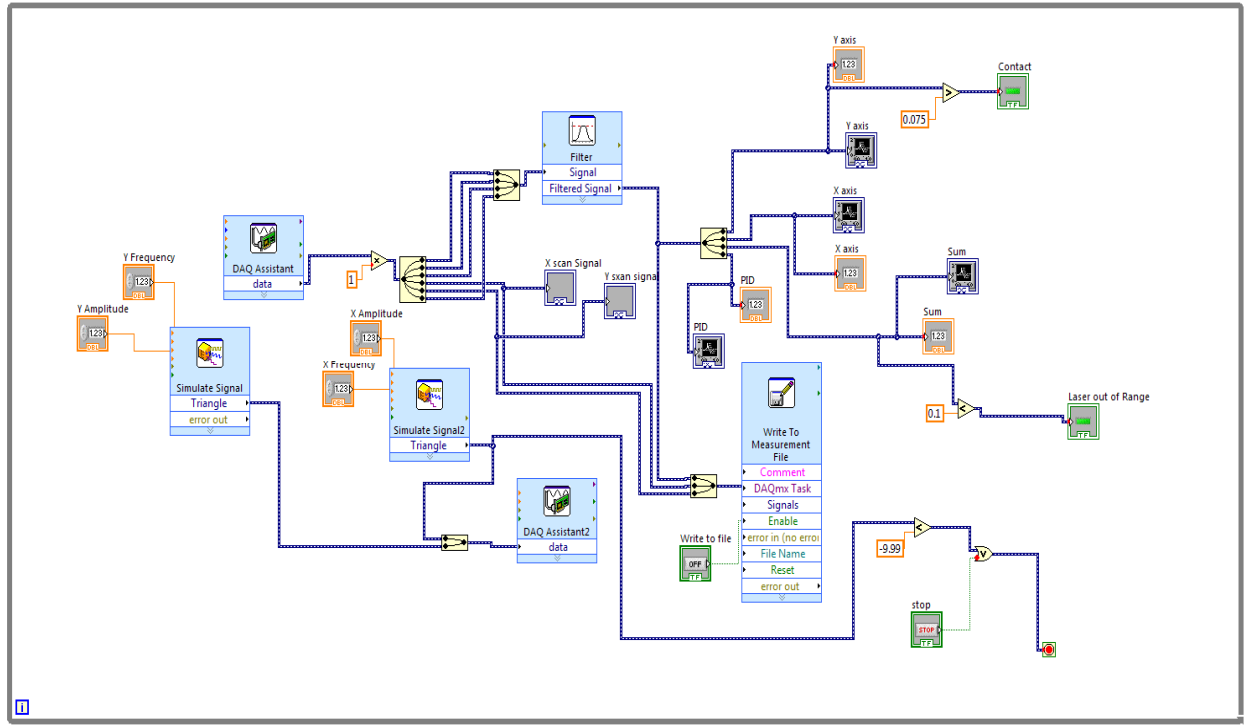
# References

- [1] Shmalz, G., Über Glatte und Ebenheit als physikalisches und physiologisches Problem. Verein Deutscher Ingenieure 1929, 1461–67.
- [2] Becker, H.; Bender, O.; Bergmann, L.; Rost, K.; Zobel, A. Apparatus for measuring surface irregularities. United States Patent number: 2728222, 1955.
- [3] Young, R.; Ward, J.; Scire, F., The topografiner: an instrument for measuring surface microtopography. Review of Scientific Instruments 1972, 43 (7), 999–1011.
- [4] Binnig, G.; Rohrer, H., Scanning tunneling microscopy. Helvetica Physica Acta 1982, 55 (6), 726–35.
- [5] M. Shusteff<sup>1</sup>, T. P. Burg<sup>1</sup> and S. R. Manalis. Measuring Boltzmann's constant with a low-cost atomic force microscope: An undergraduate experiment. American Journal of Physics 2006, 74–873.
- [6] Mitik-Dineva, N.; Wang, J.; Truong, V. K.; Stoddart, P.; Malherbe, F.; Crawford, R. J.; Ivanova, E. P., Escherichia coli, Pseudomonas aeruginosa, and Staphylococcus aureus attachment patterns on glass surfaces with nanoscale roughness. Current Microbiology 2009, 58 (3), 268–73.
- [7] Sugimoto, Y.; Pou, P.; Abe, M.; Jelinek, P.; Perez, R.; Morita, S.; Custance, O., Chemical identification of individual surface atoms by atomic force microscopy. Nature 2007, 446 (7131), 64–67.
- [8] Stipp, S. L. S., C. M. Eggleston, and B. S. Nielsen. Calcite surface structure observed at microtopographic and molecular scales with atomic force microscopy (AFM). Geochimica et Cosmochimica Acta 58.14 (1994): 3023-3033.
- [9] Gao, Guangtu, et al. Atomic-scale friction on diamond: a comparison of different sliding directions on (001) and (111) surfaces using MD and AFM. Langmuir 23.10 (2007): 5394-5405.
- [10] Giessibl, F. J., Advances in atomic force microscopy. Reviews of Modern Physics 2003, 75 (3), 949–83.
- [11] Gan, Y., Atomic and subnanometer resolution in ambient conditions by atomic force microscopy. Surface Science Reports 2009, 64 (3), 99–121.
- [12] Zhang, Q.; Archer, L. A., Interfacial friction of surfaces grafted with one- and two-component self-assembled monolayers. Langmuir 2005, 21 (12), 5405–13.

- [13] Cyganik, P.; Budkowski, A.; Raczkowska, J.; Postawa, Z., AFM/LFM surface studies of a ternary polymer blend cast on substrates covered by a self-assembled monolayer. *Surface Science* 2002, 507–10, 700–6.
- [14] Salaita, K.; Amarnath, A.; Maspoch, D.; Higgins, T. B.; Mirkin, C. A., Spontaneous ‘phase separation’ of patterned binary alkanethiol mixtures. *Journal of the American Chemical Society* 2005, 127 (32), 11283–87.
- [15] Puentes, Victor F., et al. Collective behaviour in two-dimensional cobalt nanoparticle assemblies observed by magnetic force microscopy. *Nature materials* 3.4 (2004): 263-268.
- [16] Maye, M. M.; Luo, J.; Han, L.; Zhong, C. J., Probing Ph-tuned morphological changes in coreshell nanoparticle assembly using atomic force microscopy. *Nano Letters* 2001, 1 (10), 575–79.
- [17] Boyd, Robert D., Siva K. Pichaimuthu, and Alexandre Cuenat. "New approach to inter-technique comparisons for nanoparticle size measurements; using atomic force microscopy, nanoparticle tracking analysis and dynamic light scattering." *Colloids and Surfaces A: Physicochemical and Engineering Aspects* 387.1 (2011): 35-42.
- [18] Stomp, Romain, et al. Detection of single-electron charging in an individual InAs quantum dot by noncontact atomic-force microscopy. *Physical review letters* 94.5 (2005): 056802.
- [19] Falvo, M. R.; Clary, G. J.; Taylor, R. M.; Chi, V.; Brooks, F. P.; Washburn, S.; Superfine, R., Bending and buckling of carbon nanotubes under large strain. *Nature* 1997, 389 (6651), 582–84.
- [20] Ho-Yin, C.; Ning, X.; Jiangbo, Z.; Guangyong, L. A deterministic process for fabrication and assembly of single carbon nanotube based devices, 5th IEEE Conference on Nanotechnology 2005; pp 713–16.
- [21] Jaganathan, H.; Ivanisevic, A., Heterostructured DNA templates: a combined magnetic force microscopy and circular dichroism study. *Applied Physics Letters* 2008, 93 (26), 263104–3.
- [22] Best, Robert B., et al. Mechanical unfolding of a titin Ig domain: structure of transition state revealed by combining atomic force microscopy, protein engineering and molecular dynamics simulations. *Journal of molecular biology* 330.4 (2003): 867-877.
- [23] Lyubchenko, Yuri, et al. Atomic force microscopy of long DNA: imaging in air and under water. *Proceedings of the National Academy of Sciences* 90.6 (1993): 2137-2140.
- [24] Gaboriaud, F.; Dufrene, Y. F., Atomic force microscopy of microbial cells: application to nanomechanical properties, surface forces and molecular recognition forces. *Colloids and Surfaces B: Biointerfaces* 2007, 54 (1), 10–19.

- [25] Alsteens, David, et al. High-resolution imaging of chemical and biological sites on living cells using peak force tapping atomic force microscopy. *Langmuir* 28.49 (2012): 16738-16744.
- [26] Settini, Valeria, and Giuseppe Rega. Influence of a locally-tailored external feedback control on the overall dynamics of an AFM model. *International Journal of Non-Linear Mechanics* 80 (2016): 144-159.
- [27] Semi-Automatic Tuning of PID Gains for Atomic Force Microscopes Daniel Y. Abramovitch, Storrs Hoen, and Richard Workman. *American Control Conference* 2008. 0743-1619
- [28] Eaton, Peter and West, Paul. *Atomic Force Microscopy* 2010. Oxford University Press
- [29] Giessibl, F. J.; Hembacher, S.; Bielefeldt, H.; Mannhart, J., Subatomic features on the silicon (111)-(77) surface observed by atomic force microscopy. *Science* 2000, 289 (5478), 422–25.
- [30] Taatjes, D. J.; Quinn, A. S.; Lewis, M. R.; Bovill, E. G., Quality assessment of atomic force microscopy probes by scanning electron microscopy: correlation of tip structure with rendered images. *Microscopy Research and Technique* 1999, 44 (5), 312–26.





## A2 PID Controller Code with Protocols for communication with AFM LabVIEW Interface

```

unsigned long lastTime, last=0;

double Input, Output, Setpoint, FinalOutput, MaxOutput;

double errSum, lastErr;

double kp, ki, kd;

String inString = "";

int n=0; double a;

int state = 0;

void ComputePID()
{
    unsigned long now = millis();

    double timeChange = (double)((now - lastTime));

    timeChange=timeChange/1000;

    //Compute all the working error variables

    double error = Setpoint - Input;

    errSum += (error * timeChange);

```



```

double dErr = (error - lastErr) / timeChange;

//Compute PID Output

Output = kp * error + ki * errSum + kd * dErr;

if(Output>0)
{
    if(Output>4095)
    {
        Output=4095;
    }
    FinalOutput=map(Output,0,4095,2048,4095);
}
else
{
    if(Output<-4095)
    {
        Output=-4095;
    }
    FinalOutput=map(Output,-4095,0,0,2047);
}

//Remember some variables for next time

lastErr = error;

lastTime = now;
}

void SetSetpoint(double a)
{
    Setpoint=a; //(a+0.25)*4095/0.5;
}

void SetTuning(double Kp, double Ki, double Kd)
{
    kp = Kp;
    ki = Ki;
    kd = Kd;
}

void setup() {

```

```

Serial.begin(9600);

analogReadResolution(12);

analogWriteResolution(12);

SetTuning(0.025,0,0);

analogWrite(DAC1, 2047);

Input=analogRead(A5);

SetSetpoint(1800);

pinMode(33, OUTPUT);
}

void loop() {

  //Serial communication

  while (Serial.available() > 0)

  {

    char inChar = Serial.read();

    if (inChar != '\n')

    {

      if(inChar == 'P') n=1;

      else if(inChar == 'T') n=2;

      else if(inChar == 'D') n=3;

      else if(inChar == 'S') n=4;

      else inString += (char)inChar;

    }

    else

    {

      a=inString.toFloat();

      inString = "";

    }

    if(n==1) {kp=a;}

    if(n==2) {ki=a;}

    if(n==3) {kd=a;}

    if(n==4) {SetSetpoint(a);}

    SetTuning(kp,ki,kd);

  }

  Input=analogRead(A5);

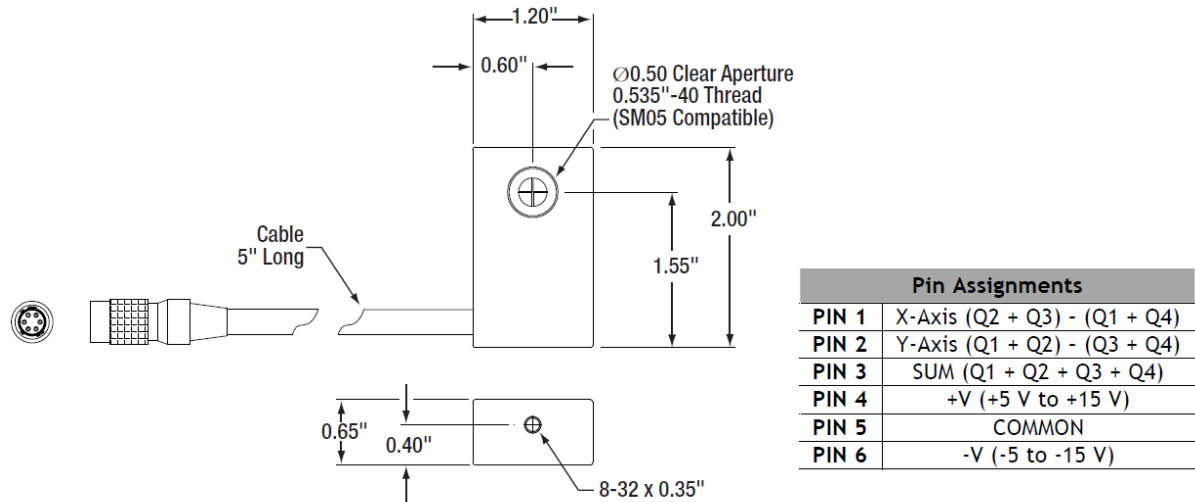
```

```
ComputePID();  
  
analogWrite(DAC1, FinalOutput);  
  
Serial.print(Input);  
  
Serial.print(',');  
  
Serial.print(FinalOutput);  
  
Serial.print(",");  
  
Serial.println(Setpoint);  
  
delay(1);
```

### A3 Matlab Code for Image Generation

```
% X is the Y axis sequential data from Photodetector  
x=x';  
img=x(1511:2510);  
n=613;  
while n<=998  
    n1=1000*(n-1)+711;  
    n2=(1000*n)+710;  
    img=[img;x(n1:n2)];  
    n=n+2;  
end  
img1=mat2gray(img);  
imshow(img1)  
imwrite(img1, 'AFMimage.jpg');
```





### B3 New Focus Piezo Linear Actuator Picomotor

<b>Travel Range</b>	12.7 mm	<b>Drive Torque</b>	0.018 Nm
<b>Minimum Incremental Motion</b>	<30 nm	<b>Cable Length</b>	2.1 m
<b>Maximum Speed</b>	1.2 mm/min	<b>Connector Type</b>	4-Pin RJ-22
<b>Axial Load Capacity</b>	22 N	<b>Rated Life</b>	> 1 x 10 <sup>9</sup> steps
<b>Mounting</b>	M12 x 0.5 mm Thread	<b>Operating Temperature</b>	10-40 C
<b>Frequency</b>	2 kHz		

B4 Newport ULTRAlign Precision XYZ Motion Stage

<b>Axes of Travel</b>	X, Y, Z	<b>Material</b>	Stainless Steel
<b>Maximum Stage Travel</b>	12.7 mm	<b>Bearings</b>	Crossed-Roller Bearings
<b>Thread Type</b>	M4 and M6	<b>Drive Location</b>	Center drive
<b>Recommended Actuators</b>	Sold Separately	<b>Maximum Centered Load</b>	156 N
<b>Load Capacity</b>	156 N	<b>Optical Axis Height</b>	98.4 mm
<b>Angular Deviation</b>	<100 $\mu$ rad		

